NONOBTUSE TRIANGULATIONS OF PSLGS

CHRISTOPHER J. BISHOP

Abstract. We show that any planar PSLG with n vertices has a conforming triangulation by $O(n^{2.5})$ nonobtuse triangles; they may be chosen to be all acute or all right. This result also improves a previous $O(n^3)$ bound of Eldesbrunner and Tan for conforming Delaunay triangulations. In the special case that the PSLG is the triangulation of a simple polygon, we will show that only $O(n^2)$ elements are needed, improving an $O(n^4)$ bound of Bern and Eppstein. We also show that for any $\epsilon > 0$, every PSLG has a conforming triangulation with $O(n^2/\epsilon^2)$ elements and with all angles bounded above by $90^\circ + \epsilon$. This improves a result of S. Mitchell when $\epsilon = \frac{3}{8}\pi = 67.5^\circ$ and Tan when $\epsilon = \frac{7}{30}\pi = 42^\circ$. Finally, we prove that any PSLG has a conforming quadrilateral mesh with $O(n^2)$ elements and all new angles between 60° and 120° (the complexity and angle bounds are both sharp). Moreover, all but $O(n)$ of the angles may be taken in a smaller interval, say $[89^\circ, 91^\circ]$.

Date: June 2010.

1991 *Mathematics Subject Classification.* Primary: 30C62 Secondary:

Key words and phrases. nonobtuse, acute, triangulation, conforming triangulation, PSLG, Delaunay, Gabriel, nearest-neighbor learning, quadrilateral mesh, beta-skeleton, thick-thin decomposition, polynomial complexity,

The author is partially supported by NSF Grant DMS 10-06309. This is a very preliminary version and should not be distributed. Please contact me for the latest version if you wish to share this with someone.

1. Introduction

A planar straight line graph (or PSLG from now on) is the union of a finite number (possibly none) of non-intersecting open line segments together with a disjoint finite set that includes all the endpoints of the line segments, but may include other, isolated points as well. See Figure 1 for some examples of PSLGs.

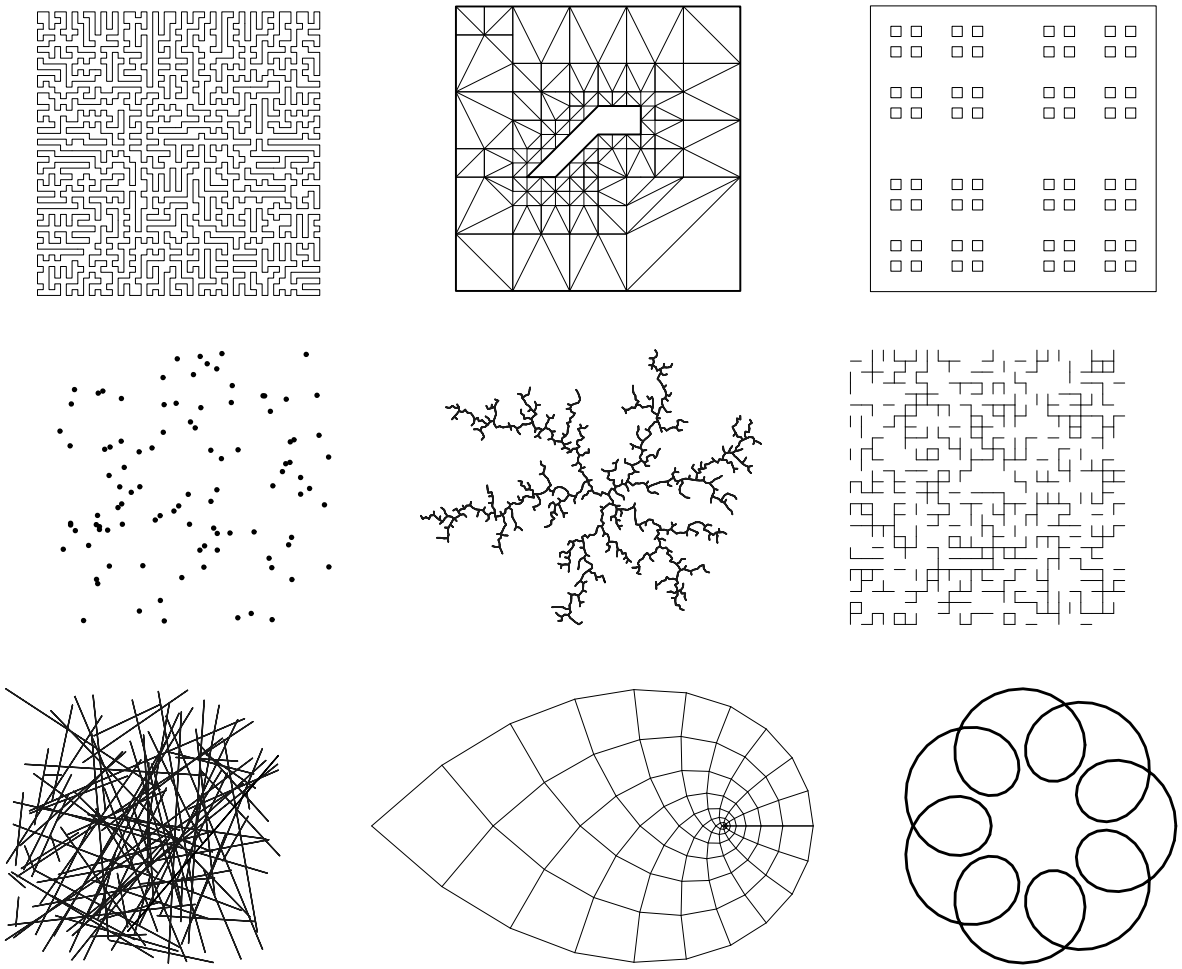

Figure 1. Some PSLGs: a simple polygon, a triangulation, a polygon with holes, a point cloud, a random tree, a percolation graph, random line segments, a structured grid and a self-intersecting 200-gon.

If Γ is a PSLG, let V be the vertices in Γ and let $n = |V|$ be the number of vertices. Suppose V' is a point set containing V. We say a triangulation of V' conforms to Γ if the edges of the triangulation cover the edges of Γ. We want to build conforming

triangulations for Γ that have small complexity (the number of elements) and good geometry (the shape of each element), but these two goals are often in conflict and we must sometimes choose which is more important in a particular situation. In this paper we are primarily interested in complexity and in proving bounds that depend on n but not on the particular geometry of Γ. This means that we cannot have a positive lower bound on angles, or an upper bound that is strictly less than 90°. Linear complexity for nonobtuse triangulations of simply polygons is already known [11], as is a quadratic lower bound for PSLGs (see [7]), but giving a polynomial upper bound for nonobtuse triangulation of PSLGs has remained open (e.g., see Problem 3 of [5]). We give such a bound by proving:

Theorem 1.1. *Every PSLG has a $O(n^{2.5})$ conforming nonobtuse triangulation. The triangles may be taken to be either all acute or all right.*

Corollary 1.2. *Every PSLG has a $O(n^{2.5})$ conforming Delaunay triangulation.*

The corollary improves a $O(n^3)$ bound of Edelsbrunner and Tan [25]. The gap between $O(n^2)$ and Theorem 1.1 can be decreased in some special cases, e.g.,

Theorem 1.3. *A triangulation of a simple n-gon has an $O(n^2)$ acute refinement.*

This improves a $O(n^4)$ bound given by Bern and Eppstein in [7]. We can also approach the quadratic lower bound if we consider "almost nonobtuse" triangulations:

Theorem 1.4. *Every PSLG has a conforming triangulation with $O(n^2/\epsilon^2)$ elements and all angles $\leq 90^\circ + \epsilon$.*

This improves a result of S. Mitchell [49] with upper angle bound $\frac{7}{8}\pi = 157.5^\circ$ and a result of Tan [61] with bound $\frac{11}{15}\pi = 132^\circ$. The next result concerns quadrilaterals rather than triangles, but the proof uses the same ideas as in Theorem 1.1:

Theorem 1.5. *Every PSLG has a conforming quadrilateral mesh with all new angles between 60° and 120° and using at most $O(n^2)$ quadrilaterals. Moreover, all but $O(n)$ of the vertices have degree four.*

The final claim implies the mesh can be partitioned into (combinatorial) rectangular grids using motorcycle graphs as described by Eppstein, Goodrich, Kim and

Tamstorf in [28]. Hence the mesh is completely described by a graph of size $O(n)$ with integer labels on the edges; the labels give the size of the rectangular pieces and the graph describes how the pieces are joined together. The 120° upper angle bound and the quadratic number of vertices in Theorem 1.5 are both sharp, but the number of large angles need not be $\sim n^2$. As an analog to Theorem 1.4 we will prove

Theorem 1.6. *For any PSLG and any $\epsilon > 0$ there is a $O(n^2/\epsilon^2)$ conforming quadrilateral mesh with all new angles between 60° and 120°, but only $O(n/\epsilon)$ elements have an angle outside $[90^\circ - \epsilon, 90^\circ + \epsilon]$.*

For example, every PSLG has a $O(n^2)$ mesh with all new angles in $[60^\circ, 120^\circ]$ and all but $O(n)$ angles in $[89^\circ, 91^\circ]$. This provides another sense in which the mesh is "mostly rectangular".

Acute and nonobtuse triangulations arise in a variety of contexts. In recreational mathematics one asks for the smallest triangulation of a given object into acute or nonobtuse pieces. For example, a square can obviously be meshed with two right triangles but less obvious is the fact that it can be acutely triangulated with eight elements but not seven, [21]. For further results of this type see [31], [32], [34], [36], [38], [39], [40], [41], [56], [70], [71], [72] and the 2002 survey [73]. There is less known in higher dimensions, but recent work has shown there is an acute triangulation of $\mathbb{R}^3$, but no acute triangulation of $\mathbb{R}^n$, $n \geq 4$ [17], [43], [45], [65], [66], [64]. In numerical methods such as the finite element method, a nonobtuse triangulation frequently gives simpler and better behaved algorithms, and often allows one to prove a discrete maximum principle. There is a large literature on such results and some examples are listed in Appendix B.

In 1960 Burago and Zalgaller [18] showed that any polyhedral surface has an acute triangulation, but without giving an estimate of the number of triangles needed. This was used as a technical lemma in their proof of a polyhedral version of the Nash embedding theorem. [19] is a 1995 sequel to this paper. In 1984 Gerver [33] used the Riemann mapping theorem to show that if all polygon angles exceed 36°, then there always exists a dissection into triangles with maximum angle 72° (in a dissection, adjacent triangles need not meet along an entire edge). In 1988 Baker, Grosse and Rafferty [2] again proved that any polygon has a nonobtuse triangulation, and their construction also gives a lower angle bound. In this case no complexity bound in

terms of n alone is possible, although there is a sharp bound in terms of integrating the local feature size over the polygon. For details, see [9], [53] or the survey [24]. Other papers that deal with algorithms for finding nonobtuse and acute triangulations include [29], [44], [46], and [48].

A linear bound for nonobtuse triangulation of point sets was given by Bern, Eppstein and Gilbert in [9], and Bern and Eppstein [7] gave a quadratic bound for simple polygons with holes (this is a polygonal region where every boundary component is a simple closed curve or an isolated point). Bern, Dobkin and Eppstein improved this to $O(n^{1.85})$ for convex domains in [4]. Bern, S. Mitchell and Ruppert [11] showed $O(n)$ works for nonobtuse triangulation of simple polygons with holes in 1994 and their construction uses only right triangles. These and related results are discussed in the surveys [5] and [12].

Maehara [47] showed that any nonobtuse triangulation with N triangles can be refined to an acute triangulation with $O(N)$ elements. A different proof was given by Yuan in [69].

Nonobtuse triangulations occur in the theory of machine learning; [55] describes a nearest neighbor learning algorithm in which a polygon is "learned" by finding two point sets E, F so that the interior of the polygon is

$$\{z \in \mathbb{R}^2 : \operatorname{dist}(z, E) < \operatorname{dist}(z, F)\}.$$

The authors of [55] show that a nonobtuse triangle can be learned with 9 points and reduce learning any simply polygon P to finding a nonobtuse triangulation of the PSLG formed by adding the boundary of the convex hull of P to P. Essentially, their method is to find a point set whose Voronoi diagram covers P. At least n^2 points are needed in some cases (see [55]) and finding the minimal size of such a point set is known to to NP-hard (see [37]). Our result, combined with the argument in [55], shows:

Corollary 1.7. *If Γ is a PSLG of size n, there is a collection of $O(n^{2.5})$ points whose Voronoi diagram covers Γ.*

A triangulation is called Delaunay if whenever two triangles share an edge e, the two angles opposite e sum to 180° or less. If all the triangles are nonobtuse, then this is certainly the case, so Theorem 1.1 immediate implies Corollary 1.2. This

implies the 1993 result of Edelsbrunner and Tan [25] that any PSLG has a conforming Delaunay triangulation of size $O(n^3)$. Conforming Delaunay triangulations for Γ are also called Delaunay refinements of Γ. There are numerous papers discussing Delaunay refinements including [24], [30], [50], [53], [54] and [59].

An alternate characterization of the Delaunay triangulation of a point set V is to require that each edge of the triangulation be the chord of an open disk that contains no points of V. A stronger requirement is that the edge be the diameter of such a disk. This is the Gabriel condition. Every edge of an nonobtuse triangulation is a Gabriel edge (see Figure 2) so Theorem 1.1 implies

Corollary 1.8. *Every PSLG has a $O(n^{2.5})$ conforming Gabriel graph.*

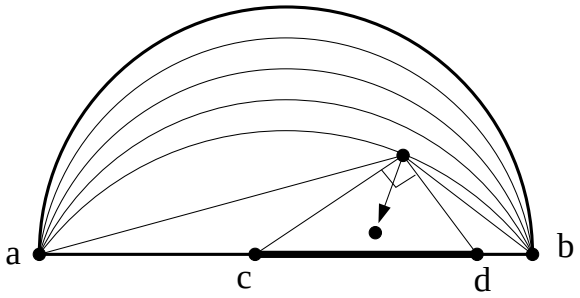

FIGURE 2. Nonobtuse triangulations have Gabriel edges. If not, some edge $I = [a, b]$ has a vertex in an open half-disk with base I. Choose the vertex v that maximizes the angle subtended by I and choose a strict subinterval $[c, d]$ that subtends angle $\pi/2$ from v. Since the triangulation is nonobtuse, there must be another vertex in the right triangle formed by v and $[c, d]$, which contradicts maximality of v.

Although stated as a corollary of Theorem 1.1, we will actually prove Corollary 1.8 first and deduce the theorem from it using the ideas of Bern, Mitchell and Ruppert from [11].

Suppose V is a finite point set and $0 < \beta \leq 1$. Let $\theta = \pi - \arcsin(\beta)$. We say that an edge e between points $v, w \in V$ is in the β-skeleton of V if the angle $\angle vpw$ is $\geq \theta$ for all $p \in V \setminus \{v, w\}$. This requires that a certain open crescent with axis e contains no points of V. See third picture in Figure 3. When $\beta = 1$, this is the same as the Gabriel condition.

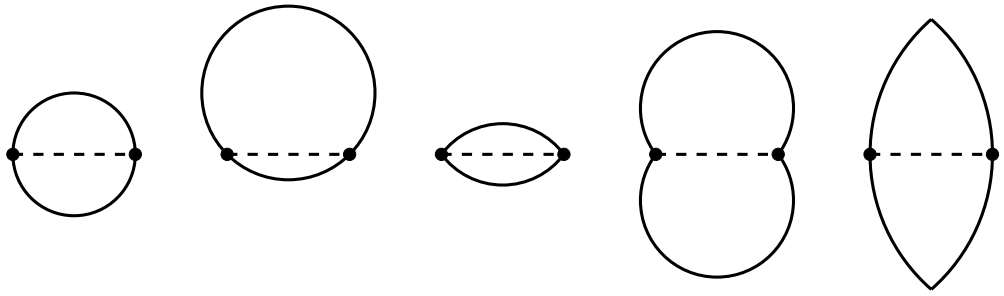

FIGURE 3. An edge (dashed) is included in the Gabriel graph if the disk with this diameter contains no other vertices. It is a Delaunay edge if it is the chord of some disk that contains no other vertices. For $0 < \beta < 1$, the edge is included in the β-skeleton if a certain crescent is empty. For $\beta > 1$ circle based skeletons require a certain union of disks to be empty and crescent based skeletons require a certain crescent to be empty.

Theorem 1.9. *For $0 < \beta < 1$, every PSLG has a conforming β-skeleton with at most $O(n^2/(1-\beta))$ vertices.*

If $\beta > 1$ then there are (at least) two different definitions of the β-skeleton in the literature: circle based and crescent based. For circle based β-skeletons the empty region is the set of points where the angle subtended by $[v, w]$ is less than $\theta = \arcsin \frac{1}{\beta}$. See [27]. This region is a union of two equal sized disks that have $[v, w]$ as a common chord. See fourth picture in Figure 3. For circle based skeletons there is no bound in terms of n alone for the number of vertices needed to construct a conforming β-skeleton (see Appendix A).

In crescent based β-skeletons, the empty region is the intersection of two disks of radius $\beta|v - w|$ with centers that lie on the line through v, w and are distance $\beta - \frac{1}{2}$ from $\frac{1}{2}(v + w)$. See the last picture in Figure 3. See [20]. It is easy to see that the diameter segment of a Gabriel disk can be subdivided into $O(\beta)$ equal subintervals that are each in the crescent based β-skeleton (see Figure 34). Thus any PSLG has a $O(n^{2.5}\beta)$ conforming crescent based β-skeleton for $1 \le \beta < \infty$.

As noted above, we can find quadratic sized triangulations with upper angle bounds as close to 90° as we want, but for quadrilateral meshes, we cannot force the maximum angle so close to 90°. In [8], Bern and Eppstein show that if P is a simple polygon with all angles $\ge 120°$ then any quadrilateral mesh of P also has an angle $\ge 120°$.

(Euler's formula implies there is either an interior vertex of degree 3 or a boundary vertex of degree 2, either of which gives an angle $\geq 120°$). They also showed that any simply polygon has a linear sized quadrilateral mesh with all angles $\leq 120°$, so this upper bound is sharp. In [14] I showed that every simple polygon has a linear sized quadrilateral mesh with all new angles between $60°$ and $120°$ and the lower bound is also sharp. More precisely, every angle in the mesh is between $60°$ and $120°$ except for angles less than $60°$ in the original polygon; these are all left unchanged. If Γ is a polygon with holes, then any bounded, connected component of the complement has an $O(n)$ quadrilateral mesh with all new angles between $60°$ and $120°$. This was proven by Chris Green in [35].

In Theorem 1.5 it is also true that angles $< 60°$ formed by edges of the PSLG are left unchanged. However, to say that all other angles lie between $60°$ and $120°$ requires a convention about what region is covered by the mesh. The most natural thing is to make the mesh fill the convex hull of Γ. If so, then the boundary of the convex hull may have small angles or may make small angles with some edges of Γ and these angles cannot be removed. We will consider these as "old angles" since they are forced to be in the mesh. All other angles in the mesh will be between $60°$ and $120°$. An alternative to meshing the convex hull is to place Γ strictly inside the interior of some simple polygon P that has no angles $< 60°$ (e.g., a big square) and have the mesh fill the interior of P. In this case, the only angles $< 60°$ in the mesh are formed by angles of Γ.

Why is nonobtuse triangulation for PSLGs more difficult than for simple polygons? Roughly speaking, the problem is that adding a new vertex often forces a new edge, which, in turn, produces a new vertex. Thus vertices "propagate" until they run into the boundary or an existing vertex. A couple of examples illustrate the problems that arise. In Figure 4, the left picture shows a PSLG that is already acutely triangulated. On the right we add a single new vertex (the black dot). However, to nonobtusely triangulate the new PSLG requires adding many more lines (the dashed triangulation drawn is not necessarily optimal; can the reader do better?). Figure 5 shows the problem that arises when we want to simultaneously triangulate the inside and outside of a polygon P. We first nonobtusely mesh the inside, but this may create new vertices on P. Then we mesh the outside incorporating these new points, but create even

more vertices on P. This forces us to remesh the interior to incorporate the new vertices. Can we nonobtusely mesh the inside and outside using exactly the same set of vertices on P? In this paper we show that this is possible.

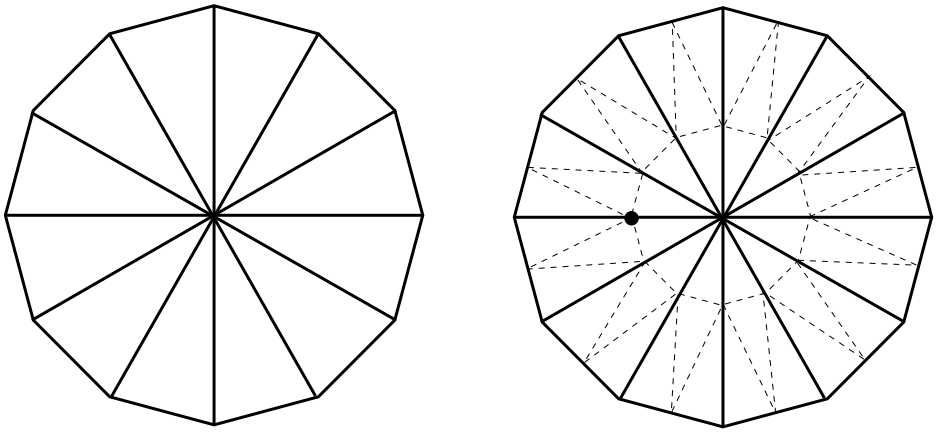

FIGURE 4. Small changes to a PSLG (such as adding a single vertex) can require large changes to the triangulation.

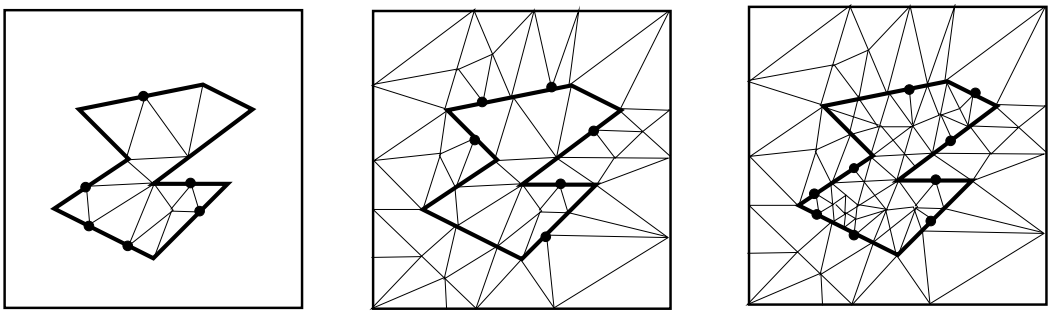

FIGURE 5. Naively triangulating two sides of a polygon one at a time creates new vertices (black dots) at each stage, which force another refinement of the other side. Can we eventually mesh one side without creating new vertices on the polygon?

The rest of the paper is organized as follows:

Section 2: We prove triangulation of a simple n-gon has an acute refinement with $O(n^2)$ elements. The proof of this introduces the framework for the rest of the paper and shows that finding a nonobtuse triangulation reduces to finding a certain kind of conforming Gabriel graph.

Section 3: We define thin regions and propagation paths.

Section 4: We define return regions and show there are only $O(n)$ such regions.

Section 5: We consider bendings of propagation paths that preserve the Gabriel property and estimate how far we can bend a path.

Section 6: We build traps in each return region.

Section 7: We complete the proof of Theorem 1.1.

Section 8: We prove Theorems 1.4 and 1.9.

Section 9: We use a result of David Eppstein to connect components of a disconnected PSLG without adding small angles.

Section 10: We review the thick/thin decomposition for polygons from [13].

Section 12: We prove Theorem 1.5 except for the construction of certain special meshes called sinks.

Section 13: We construct the sinks.

Section 14: We pose questions for further research.

Appendix A: We give lower bounds for the problems we consider.

Appendix B: We give some references in the numerical analysis literature where acute and nonobtuse triangulations arise naturally.

2. Acutely refining a triangulation

To give an introduction to the rest of this paper, we start by proving Theorem 1.3. The proof of this is a "warm-up" for the the proof of Theorem 1.1 and offers an opportunity to review important facts from [11] and [69] that we will use (and slightly modify in a few cases).

Let $\mathcal{T}$ be some collection of triangles in the plane. Suppose we have a equivalence relation on the collection of edges and assume that each equivalence class has one or two elements; in the latter case both edges must have the same length and are identified by an isometry. The space X obtained by taking the disjoint union of the triangles with their edges identified as above will be called a triangulated surface. Its boundary, ∂X, consists of all edges that are not identified with another edge. The identified edges are called interior edges of the triangulation.

Theorem 2.1. *Any finite triangulated surface can be nonobtusely triangulated with either all acute or all right triangles.*

This is not a new result and can be proven in various ways going back at least to Burago and Zalgaller in [18]. The proof we give here, however, can be adapted to give estimates of the number of triangles needed. Theorem 1.3 will be an immediate corollary and Theorem 1.1 will follow from more extensive modifications.

A sector is a region in the plane that is similar to $\{re^{i\theta} : r_1 < r < r_2, 0 < \theta < \theta_0\}$ where $0 \le r_1 < r_2 < \infty$ and $0 < \theta_0 \le 2\pi$. Each sector has two straight sides and either one or two circular arc edges (depending on whether $r_1 > 0$ or $r_1 = 0$). When we have to distinguish these two cases we will call the $r_1 = 0$ case a "proper sector" and the $r_1 > 0$ case a "truncated sector". The meeting point of the lines containing the straight sides is called the vertex of the sector and θ_0 is the angle of the sector. Every sector has two obvious orthogonal foliations: the E-foliation by circular arcs concentric with the vertex and the N-foliation by radial line segments (E for "equidistant"; the leaves stay a constant distant apart and N for "normal to E"). The straight sides of a sector will be called the N-sides (since they lie in the N-foliation) and the curved sides will be called the E-sides. See Figure 6.

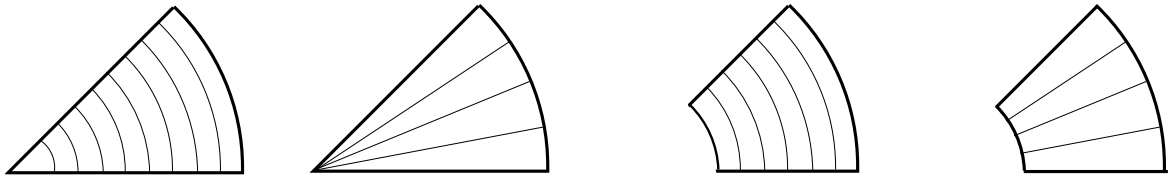

FIGURE 6. Proper and truncated sectors with E and N foliations.

We begin the proof of Theorem 2.1 by dividing each triangle T into three disjoint proper sectors (called the thin parts) whose vertices are the vertices of T, and the remaining central region (called the thick part) as illustrated in Figure 7.

The center of the inscribed circumcircle C for T is also the meeting point of the three angle bisectors. If we take circles centered at the vertices of T and meeting T where C hits T, then these circles are pairwise tangent and the tangent lines also meet at the center of C. Removing these three disks from T leaves a shaded central region that meets each side of T at a single point. However, for the current proof we remove strictly smaller sectors, so that the central region meets T in segments of positive length called the central segments. The central segments are chosen to be short enough so that the three half-disks in T with these segments as bases are

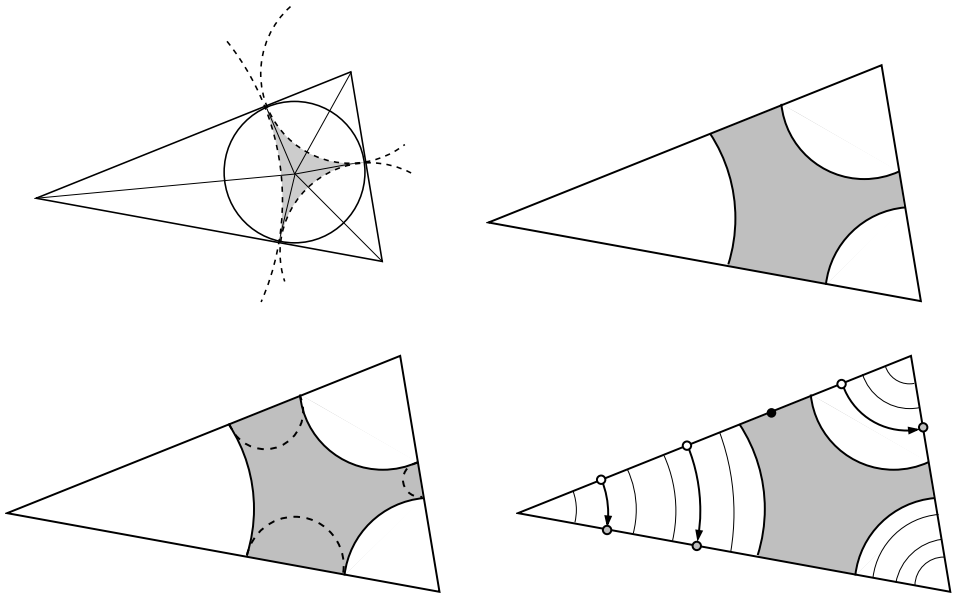

FIGURE 7. We divide a triangle into three thin parts and one thick part. We choose the thick part to hit the triangle in segments that have positive length, but are short enough so that the corresponding half-disks in T are disjoint. Points on each side are either stopping points or can be propagated to another side of T along the E-foliation.

disjoint. See Figure 7. The endpoints of the central segments are called the vertices of the thick part.

A point is called a stopping point if it is either on ∂X or is on a central segment of some triangle. Given any point in any thin part there is an E-leaf containing it. Where the E-leaf meets the boundary of the triangle, it either hits a stopping point or it can be continued into a thin part of an adjoining triangle.

Lemma 2.2. *Every E-path is either a closed loop or has two endpoints that are stopping points.*

Proof. Let ϵ be the length of the smallest stopping segment in X. Suppose γ is a propagation path that never stops and suppose that γ hits an edge e twice at points x, y within an interval of length $< \epsilon$ and that x is the first of the two points to be hit (γ has a natural direction starting from its initial point). Consider the propagation path γ_x starting at x with the same direction at γ and the parallel path γ_y starting at y. Since the paths are $< \epsilon$ apart and neither ever hits a stopping point, they must

encounter exactly the same sequence of thin parts. This means the paths stay the same distance apart forever.

If γ crossed e at x and y in opposite directions then γ_x and γ_y must meet half-way between x and y on γ, which contradicts the observation that they remain a constant distance apart. Thus γ crosses e at x and y in the same direction. Eventually the path from x reaches y and the path from y reaches a new point z so that $|z-y| = |y-x|$. Either $z = x$ or $z \neq x$. In the first case γ is a closed loop and so hits e only finitely often. In the second case we can repeat the construction forever, obtaining an infinite number of distinct, equally spaced points on e; an obvious impossibility. Thus if γ hits e at two points within ϵ of each other, it must be a closed loop, indeed, must be the boundary of a Möbius strip embedded in the surface. □

Thus propagating the $O(n)$ vertices of the thick regions gives $O(n)$ terminating propagation paths. These paths cut the thin part W of X into $O(n)$ tubes. Each tube has a fixed width and the intersection of each tube with a N-segment is the diameter of a disk contained in the tube. The ends of the tubes are segments in the boundaries of the thick pieces (or the boundary of the triangulation) and hence disks with these segments as diameters do not contain any vertices. Thus intersection points of the propagation paths with the triangulation edges cut the triangulation edges into Gabriel edges. See Figures 8 and 9.

Next we want to turn this collection of Gabriel edges into a nonobtuse triangulation. This part of the argument closely follows the arguments of Bern, Mitchell and Ruppert in [11]. For the convenience of the reader (and because we want to make a few changes to their arguments) we will describe the process in detail.

For a fixed triangle, the propagation paths (including endpoints) break the edges of T into finitely many segments $\{I_j\}$. At each vertex of T there are two adjacent segments of equal length, i.e., these are radii of a circle centered at the vertex. Remove the corresponding sectors from T. Also remove the half-disks in T with diameters $\{I_j\}$. What remains of T is bounded by circular arcs. See the last picture in Figure 9. These arcs must be tangent where they meet on the boundary of T, but may overlap at intersections points inside T.

Near each point where two bounding circular arcs meet we add a small disk whose interior is disjoint from all the other disks and that is tangent to the two touching

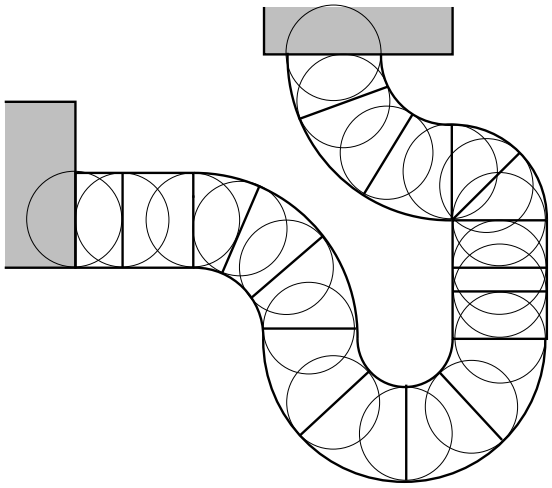

FIGURE 8. The tube edges remain a fixed distance apart and are filled by disks tangent to the sides of the tube. In particular, every intersection of a side of a thin piece with a tube is a Gabriel edge.

disks (these may be either tangent or overlapping). See the bottom left picture in Figure 9. This forms a 3-sided region that is is bounded by circular arcs. Following [11] we call this a 3-gap. These new disks are called protecting disks since they insure that all the original intersection points between disks are on the boundaries of a 3-gaps. When we have finished adding these protecting disks, all the remaining regions (those that are not 3-gaps) are bounded by tangent circular arcs and none has a boundary that intersects the boundary of T. See Figure 9.

Suppose one such connected region is bounded by K arcs. By the arguments of [11] we can add $O(K)$ new disks so that the remaining regions R are all bounded by either 3 or 4 tangents circular arcs (called 3-gaps and 4-gaps). The augmented region R^+ consists of R and the sector of the bounding disks defined by the boundary arcs. The triangle is the union of the augmented regions of all the 3-gaps and 4-gaps it contains. See Figure 10.

Theorem 2.3 (Bern-Mitchell-Ruppert, [11])**.** *Suppose R is a 3-gap or 4-gap and let R^+ be the corresponding augmented region. Then R^+ can be triangulated by at most 28 right triangles so that no new vertices are added to the boundary of R^+. Alternatively, we can use nonobtuse triangles that satisfy*

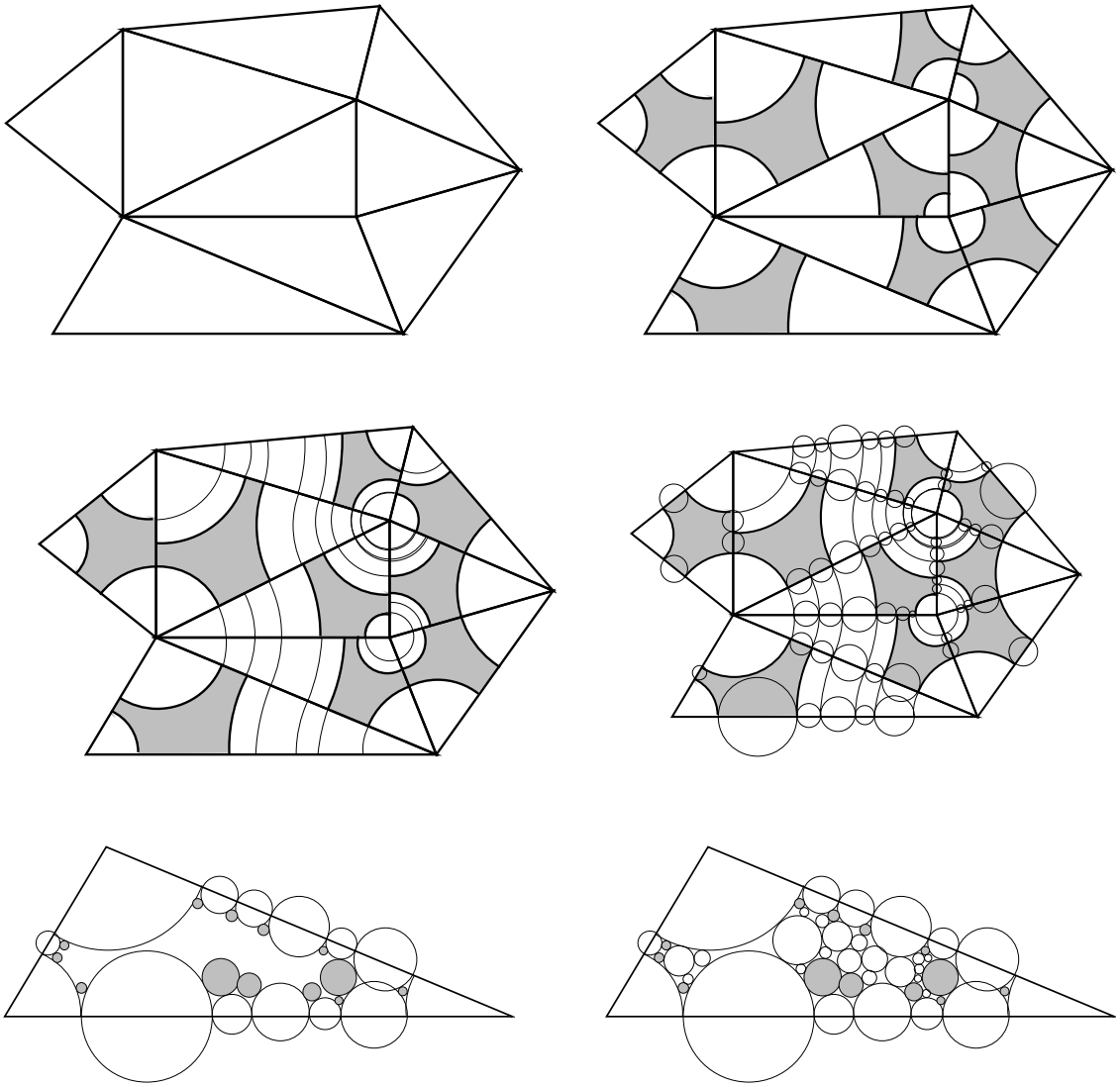

FIGURE 9. Divide each triangle into thick (shaded) and thin (white) parts and propagate the vertices until they reach a stopping point. The bottom pictures show what happens next in a single triangle T. We keep an arc at each vertex and the Gabriel disks along the boundary of T. The left picture shows the added protecting disks (shaded); this insures the boundary of T is covered by augmented regions of 3-gaps. Also note that where two boundary disks overlap, the common chord lies on a line that separates the centers of the circle (this will be used later). On the right we add disks until only 3-gaps and 4-gaps are left.

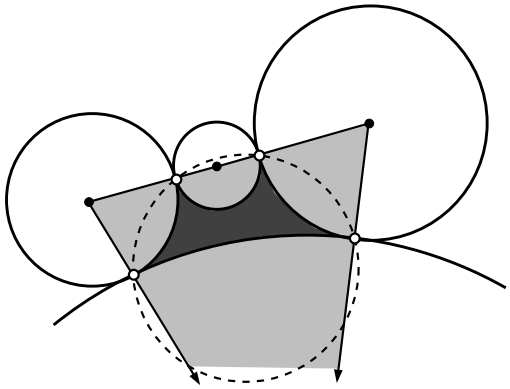

FIGURE 10. Given a region R bounded by tangent circular arcs (dark shading), the augmented region R^+ (all shading) consists of R together with the sector of each circle defined by the arc on the boundary of R (the convex hull of the arc and the center of the circle).

(1) *Any two right triangles that share an edge share an edge of the the same type (either leg-leg or hypotenuse-hypotenuse).*
(2) *Any right triangle that has a side on ∂R^+ has only one side on ∂R^+ and that side is its hypotenuse.*

The first claim is proven in [11]. The alternative conclusion will be useful later when we want to refine our nonobtuse triangulation to an acute triangulation, and requires only a few minor changes (we will add a few extra right triangles and convert a few right triangles to acute triangles). We sketch these changes below.

Proof. The first change is in triangulating 3-gaps. In [11] the center of the inscribed circle of R^+ is connected to the centers of the circle and to the points of tangencies between the circles. This gives six right triangles whose legs lie on the boundary of R^+. However, condition (3) does not hold, so we add the three chords connecting the points of tangency, and get twelve right triangles so that only hypotenuses lie on ∂R^+. Moreover, adjacent triangles only shared edges of the same type, as desired. See Figure 11.

Before triangulating 4-gaps, recall that the four vertices all lie on a single circle. This is Lemma 3 of [11]. That lemma also states that the angle measure of the four boundary arcs sums to 2π, so that at most one of the arcs can be reflex (have angle measure $> \pi$).

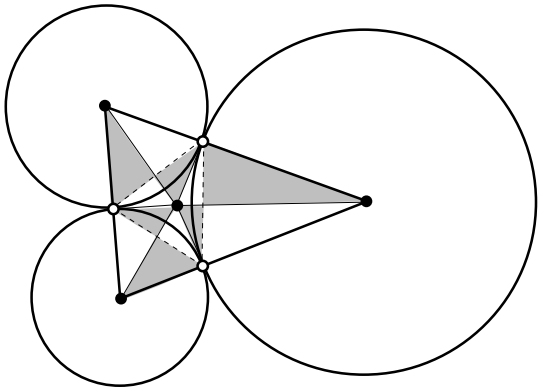

FIGURE 11. The triangulation of 3-gaps in [11] uses six right triangles, but has legs on ∂R^+. We add the dashed triangle to form twelve right triangles with only hypotenuses on ∂R^+. The reader should verify that the central dot is indeed inside the dashed triangle.

In [11] the 4-gaps are split into several cases. The first occurs when:

(1) R is centered, that is, the center of the circle C_* passing through the four points of tangency is inside the convex hull of these points and,
(2) none of the arcs in ∂R is reflex.

If both these conditions hold, then the triangulation given in [11] has the desired properties (R^+ is divided into kites by connecting the center of C_* to the four tangent points. Each kite is triangulated by adding its diagonals). See Figure 12.

The next case is when one of the four arcs is reflex. Suppose C_3 is the circle with the reflex arc and it is opposite C_1. The authors of [11] insert a new disk C_5 centered on the segment connecting the centers of C_1 and C_3 and tangent to both. This creates two new 4-gaps, neither with an reflex arc, since they both contain an arc of measure π. However, the new disk may intersect one of the other two. See Figure 13. However, the fact that the new disk is on the segment connecting the centers of C_1 and C_3 means that if it intersects, say, C_2, then the common chord of C_5 and C_2 separates the centers of C_5 and C_2. The proof of this is left to the reader. Similarly if it intersects C_4. This chord-separated property implies the associated augmented region can be triangulated by sixteen right triangles as shown on the left of Figure 14.

However, some of the right triangles on the left side of Figure 14 have legs on ∂R^+. We will fix this by making these triangles acute. Suppose the circles are

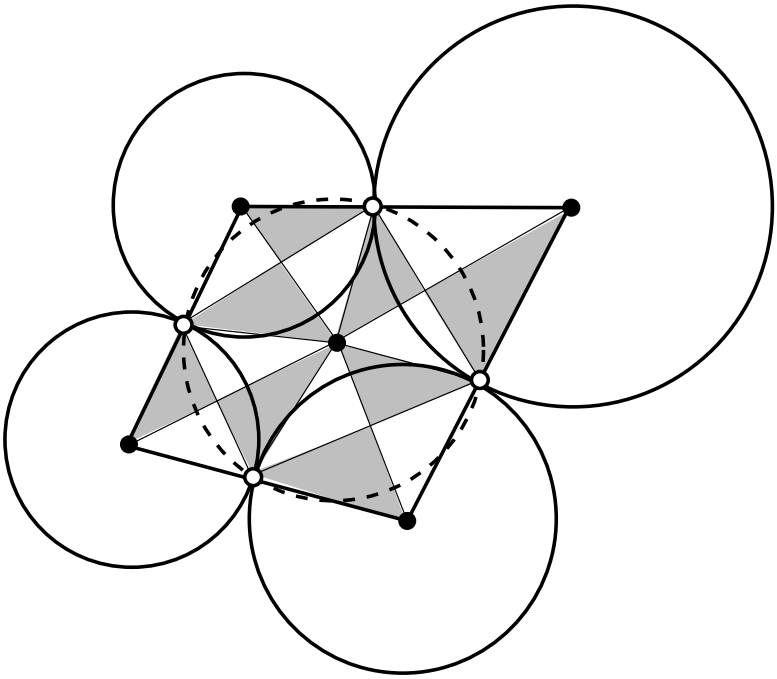

FIGURE 12. If R is centered and every arc is non-reflex, then R^+ is a union of sixteen right triangles with the desired properties.

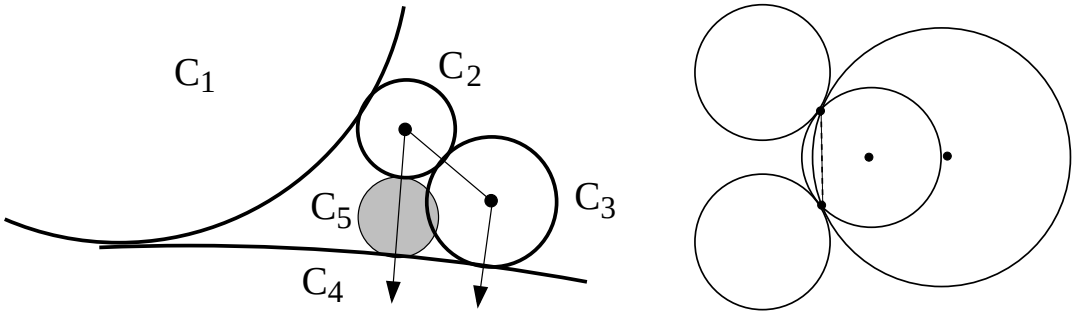

FIGURE 13. If R reflex, then add an extra disk (shaded) centered on the segment connected the non-reflex circle to its opposite. If this disk intersects one of the two other disks bounding the region, the line containing the common chord must them separate the centers of the overlapping circles. The picture on the right shows that the chord need not separate the centers in general.

C_1, C_2, C_3, C_4 with C_2, C_4 intersecting at points x, y and let c_1, c_2, c_3, c_4 be the centers of the corresponding circles. If C_2 and C_4 have equal radius, then c_1, c_3 both lie on the line through c_2, c_4. If C_2 has smaller radius than C_4, then both c_1, c_3 are closer

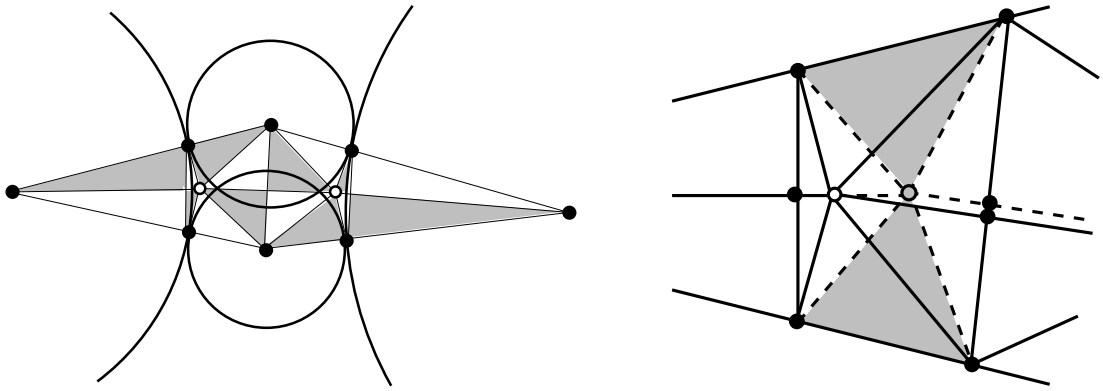

FIGURE 14. A non-reflex but overlapping 4-gap. On the left is the triangulation from[11]. We modify this by sliding the white points to make some of the right triangles acute (these are shaded in the enlargement on the right). The remaining right triangles only have hypotenuses on the boundary of the augmented region.

to c_2 than they are to c_4. Thus both c_1, c_2 lie of the same side of the line bisecting c_2, c_4, i.e., the line containing x and y. Similarly, if C_2 has larger radius than C_4, both c_1, c_3 lie on the same side of this line.

Let v_1, v_3 be the vertices of degree six in the triangulation (the white dots in Figure 14). Slide v_1 by amount $\epsilon > 0$ on the ray from c_1 through v_1 away from c_1. This gives a new point v_1'. Slide v_3 on the ray from c_3 through v_3 away from c_3 to get a point v_3'. The distance we slide v_3 is chosen so the segment $[v_1', v_3']$ is parallel to $[v_1, v_3]$. For any small enough ϵ this makes the four right triangles with legs on ∂R^+ acute and leaves all the remaining triangles right. Moreover, ∂R^+ now only contains hypotenuses of right triangles and any two adjacent right triangles share an edge of the same type.

The final case is when all the arcs of the 4-gap have angle $\leq \pi$, but the center of the circle defined by the four tangent points is not in the convex hull of these points. The authors of [11] show that a fifth disk can be added, tangent to two opposite circles, creating two new centered 4-gaps (one possibly self-intersecting) and such that the union W of the two augmented regions can be written as a union of seven kites, and each is triangulated by its diagonals. This causes the boundary of W to contain only hypotenuses and for all adjacencies to be of matching type. See Figure 15. This completes the proof of Theorem 2.3. □

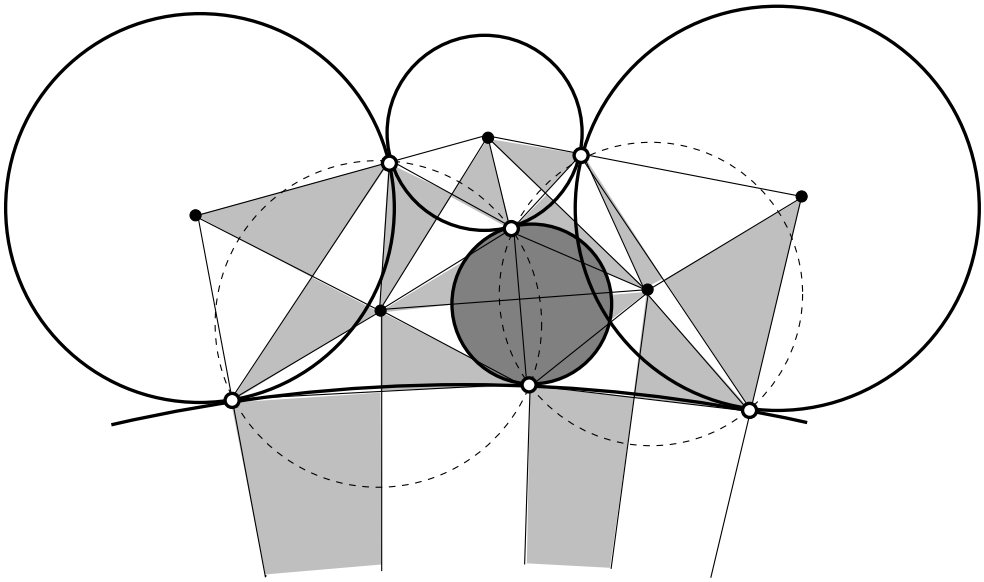

FIGURE 15. A non-centered 4-gap is split into two centered 4-gaps by the shaded disk. It is proven in [11] that such a disk exists and we use the same triangulation as given there.

The argument so far produces a nonobtuse triangulation of a triangulated surface. To refine it to an acute triangulation we use an idea of Yuan from [69]:

Theorem 2.4. *Let T be a right triangle. Form a 12-gon P by adding the midpoints of each edge of T and then adding the midpoints of each of the resulting 6 sides. This polygon has a triangulation by 24 triangles: 22 acute and 2 right triangles. The two right triangles T_1, T_2 contain the two acute angles of T. For any small enough $\epsilon > 0$, the entire triangulation can be made acute by sliding two vertices of P by ϵ along the sides of T. Either we can slide the vertices of T_1, T_2 that lie on the hypotenuse of T by ϵ towards the acute vertices of T, or we can slide the vertices of T_1, T_2 that lie on the legs of T by ϵ away from the acute vertices of T.*

Proof. The proof is basically a series of pictures; see Figure 16. Divide T into a rectangle and two right triangles by connecting the midpoint of the hypotenuse to the midpoints of the legs. Then repeat this in the two triangles. Acutely triangulate the large rectangle as shown. Then move the marked interior vertices as shown in the top of Figure 16. This makes all the triangles acute except for the two containing

the acute angles of T. These can be made acute by sliding vertices as described in the theorem (see bottom of Figure 16).

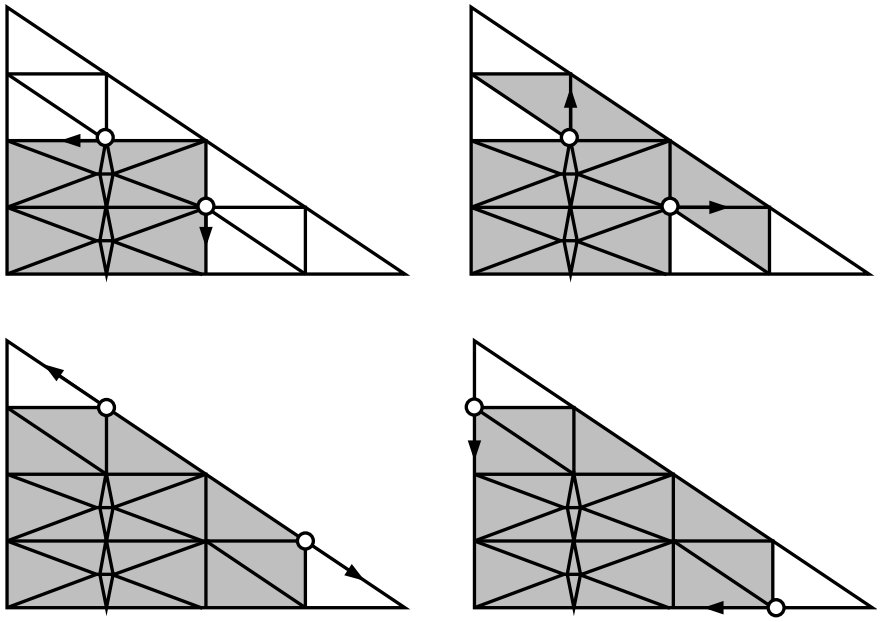

FIGURE 16. The proof of Yuan's theorem. The shaded triangles in each picture are acute. Moving the white dots in the indicated directions makes the incident right triangles acute; a small move leaves acute triangles acute.

□

Corollary 2.5. *Any nonobtuse triangulation in which adjacent right triangles only share edges of the same type (leg or hypotenuse) has an acute refinement with at most 24 times as many triangles.*

Proof. First subdivide every triangle by connecting the midpoints of each side. Subtriangles of right triangles are right and subtriangles of acute triangles are acute. Then repeat the midpoint subdivision on each resulting triangle. This gives an nonobtuse refinement of the original nonobtuse triangulation. To make it an acute triangulation we "fix" all the right triangles by sliding vertices as described in Theorem 2.4. If the edge where we slide is shared with an acute triangle, choose ϵ so small that it remains acute. If the edge is shared with another right triangle, the shared edge must be of

the same form (leg or hypotenuse), so sliding in one direction fixes both triangles at once. □

This proves Theorem 2.1 because if X is a triangulated surface, we have constructed a nonobtuse triangulation in which any adjacent right triangles share edges of the same type. This is immediate if the adjacent right triangles are in the same augmented region. Otherwise the common edge must be on the boundary of one of the original triangles, and hence is on the boundary of an augmented region, and hence must be a hypotenuse.

Corollary 2.6. *Suppose X is a triangulated surface. Suppose the dual graph of X is a tree. Then X has an acute triangulation with $O(n^2)$ elements. This occurs if X is the triangulation of a simple planar polygon, so this implies Theorem 1.3.*

Proof. If the dual is a tree, then the propagation paths can never return to the same triangle twice. Hence each propagation path generates at most $O(n)$ new vertices and there are only $O(n)$ such paths (at most 6 per triangle). □

3. Thin Regions and Tubes

Next we start on the proof of Theorem 1.1. For this result it is enough to replace a PSLG with a triangulation of itself; the number of vertices does not increase and anything that conforms to the triangulation will also conform to the original PSLG (every PSLG can be triangulated in time $O(n \log n)$, see [6]). However, the replacement may introduce new angles that are small compared to angles already present in Γ. This makes no difference for Theorem 1.1, but when we want to apply the similar ideas to prove Theorem 1.5 on quadrilateral meshes, we must avoid adding new small angles. In Section 12 we will show how to embed any PSLG Γ in a connected PSLG so that no new angles $< 60^\circ$ are created, but the complementary components will be polygons rather than triangles. In order to include this case in the current discussion, we need to generalize the discussion of thin parts slightly.

Given a connected Γ, let $\{\Omega_j\}$ denote the bounded complementary components. (The reader who is only interested in Theorem 1.1 may assume these are all triangles.) Each Ω_j has a decomposition into thick and thin parts. For triangles, this is exactly as described before; each thin part is a proper sector associated to a vertex of a

triangle. For more general polygonal regions, the thin parts may be either proper or truncated sectors. As with triangles, the proper sectors are associated to vertices of the polygon. The truncated sectors are associated to certain pairs of non-adjacent of edges (see Lemma 10.1). In either case, each thin part has an E-foliation consisting of circular arcs concentric with its vertex and the orthogonal N-foliation by segments. In the general case we also allow rectangles to occur as thin parts (think of them as truncated sectors of angle 0 and vertex ∞). In this case both foliations consist of line segments. Abusing notation slightly, we will still refer to the segments in the E-foliation as circular arcs to simplify the discussion.

We let W denote the union of all the thin parts of all the Ω_j's and call this the thin region. If Γ has n vertices then there are at most $O(n)$ thin parts in W. Clearly W is foliated by piecewise circular arcs (some of which might be line segments in the general case, as noted above) consisting of the E-leaves in each thin part. We call this the E-foliation of W. Similarly, W has an orthogonal N-foliation consisting of line segments. A connected arc on a leaf of the E-foliation will be called an E-path. A connected arc of the N-foliation is always a straight line segment, and we will call these N-segments. A maximal path is called a leaf of the foliation.

Each connected component of W is a Jordan domain that consists of straight segments in Γ and piecewise circular arcs in the complement of Γ. We let $\partial_N = \partial W \cap \Gamma$ and call this the N-boundary of W. The rest of ∂W is called the E-boundary of W and is denoted $\partial_E W$.

We say that two paths I, J in the E-foliation are parallel if for every $x \in I$ there is a $y \in J$ so that the segment $[x, y]$ is contained in an N-segment. If this is the case then the distance $|x - y|$ is the same for every pair. This is obviously true for each thin piece and the general case follows immediately.

A tube is a region that a union of two parallel E-paths and all the N-segments with endpoints on these paths. It plays the role of a rectangle if we think of the E and N foliations as defining horizontal and vertical directions. A tube's boundary is divided into four arcs: two E-paths and two N-segments. These will be called the E-sides and the N-sides of the tube. The width of the tube is the common length of the N-sides. The length L of the tube is the length of the shorter E-side of the tube.

This can be zero, even if the tube has nonempty interior, if the tube is the union of proper sectors with the same vertex (hence is a proper sector itself).

When an E-path crosses from one thin part to the next, the tangent direction is perpendicular to corresponding N-segment from both sides, so E-paths are actually C^1. Thus a directed E-path γ has a well defined change in the tangent direction between its endpoints. When γ crosses a thin piece of angle θ, we define the change in direction to be $+\theta$ if the corresponding vertex is on the left of the path and is $-\theta$ if the vertex is on the right. Note that two parallel directed E-paths must have the same change in tangent direction. Also, if we reverse the direction of a path, the change in direction changes sign.

Suppose S is a tube with N-sides $[a, b]$ and $[c, d]$ so that a and c are connected by an E-side and so are b and d. Let γ_t be the E-path in D that connects $(1-t)a+tb$ to $(1-t)c+td$. Thus γ_0 is the E-side connecting a to c and γ_1 is the E-side connecting b to d. We assume the vertices are labeled so that the tube is on the left of γ_0 as we go from a to c. Let θ denote the change in direction for γ_0 as it goes from a to c (it would be the same for any γ_t since they are all parallel).

Lemma 3.1. *With notation as above, $\ell(\gamma_t) = \ell(\gamma_0) - t\theta$.*

Proof. This is obvious for sectors and the general case is just a sum of sectors. □

The E-path that connects the midpoints of the two N-sides will be called the mid-path of the tube and its length is denoted $L_{1/2}$. The lemma implies $\ell(\gamma_t)$ is an affine function of t and hence $\ell(\gamma_t) = (1-t)\ell(\gamma_0) + t\ell(\gamma_1)$. See Figure 17. In particular,

$$L_{1/2} = \ell(\gamma_{1/2}) = \frac{1}{2}(\ell(\gamma_0) + \ell(\gamma_1)) \geq \min(\ell(\gamma_0), \ell(\gamma_1)) = L. \tag{3.1}$$

Given two parallel E-paths, we can continue them until the first time they fail to be parallel. This can happen either because one of the paths ends (i.e., it hits $\partial_N W$) or they become separated by a component of ∂W; in this case there is a last connecting segment $[x, y]$ with $x, y \in W$, and $[x, y]$ contains a component of $\partial_N W$. There are only finitely many such components of $\partial_N W$, so there is a minimal length ϵ_0 for such a component. Thus if two parallel paths in the E-foliation are less than ϵ_0 apart, they cannot stop being parallel unless one of them terminates on $\partial_N W$. Thus the argument we gave in the last section to prove propagation paths terminate also shows:

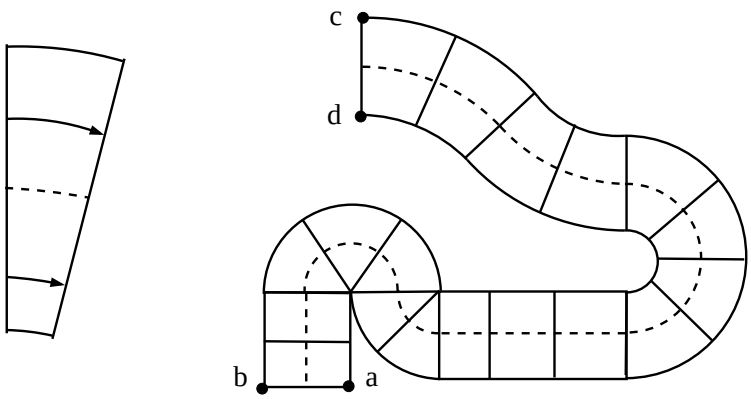

FIGURE 17. In a sector, the length of an E-leaf is a multiple of its radius, hence is linear. For a general tube, the length of γ_t is a sum of lengths in each sector so is affine in t. Here the midpath is shown as a dashed curve.

Lemma 3.2. *Every E-path is either a closed curve or has two endpoints on $\partial_N W$.*

4. Return Regions

The idea for proving Theorem 1.1 is to propagate all the vertices of the thick parts along the E-foliation until then terminate on ∂W. This cuts Γ into Gabriel segments and we obtain a nonobtuse triangulation as in Section 2. The main problem is bounding the number of Gabriel edges. There are $O(n)$ vertices and $O(n)$ thin parts, so if each propagation path only hit each thin part once, we would create only $O(n^2)$ new vertices which gives Theorem 1.1 with a $O(n^2)$ bound. However, it is possible for the propagation paths to twist and turn and to cross the same thin part arbitrarily many times. See Figure 18 for examples of how this can happen. To prove Theorem 1.1 is a geometry independent bound we must "bend" the propagations paths so that the terminate more quickly, while maintaining the Gabriel condition. We will show we can terminate every path before it crosses $O(n)$ thin parts, although we will have to add $O(n^{1.5})$ new vertices to do this, giving the $O(n^{2.5})$ bound in the theorem.

This plan will take several sections to accomplish. In this section we will describe "return regions" in W that every sufficiently long E-path must enter. In the following sections we will describe how to "bend" the propagation paths inside the return regions so that their intersections with Γ still define Gabriel edges, but so that each path only crosses each thin part a bounded number of times.

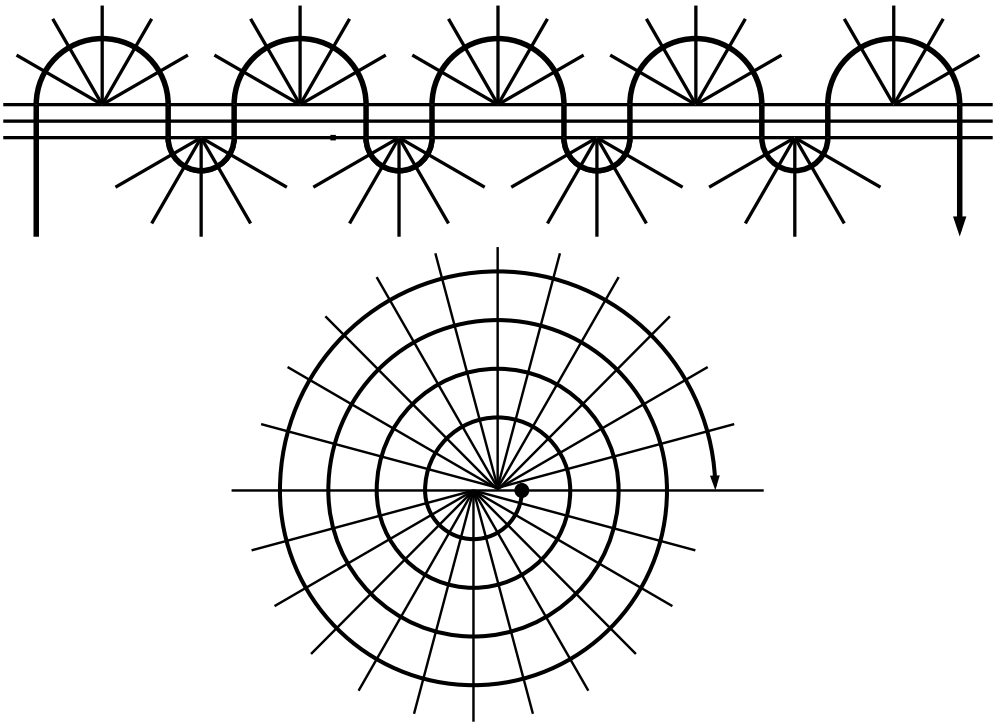

FIGURE 18. Two ways in which propagation paths can recross the same thin parts many times. The bottom picture shows a spiral; a propagation path in a sprial can hit the same edges arbitrarily often.

We start with the following simple fact (the proof is left to the reader):

Lemma 4.1. *Suppose I is a line segment and γ is a C^1 Jordan arc in the complement of I with both endpoints in the interior of I and normal to I at both endpoints. Then the total change in the tangent direction along γ has absolute value $\pi, 2\pi$ or 3π.*

Suppose I is an N-segment and γ is an E-path with both its endpoints on I and no other points on I. We call this a simple returning curve for I. We call γ a U-curve, G-curve or C-curve depending on whether the total change in direction has absolute value $\pi, 2\pi$ or 3π respectively. Now suppose γ is an E-path with its endpoints on I and also one interior point on I. Suppose that neither of the proper subpaths that are simple I-paths is a G-curve or C-curve. Then they must both be U-curves. If we give then consistent directions (the initial point of one is the terminal point of the other), then either the change of direction has the same sign for both paths or it has different signs. The first case we call a G-curve (or a G-curve of the second type if we

ever need to distinguish it from the previous sort). The second case we call a S-curve. See Figure 19. Thus any E-path that hits I three times contains subpath that is a return curve for I. Thus if $m = O(n)$ is the number of thin parts, any E-path that crosses $2m+1$ thin parts must hit some N-segment three times and must contain one of the type of return paths described above.

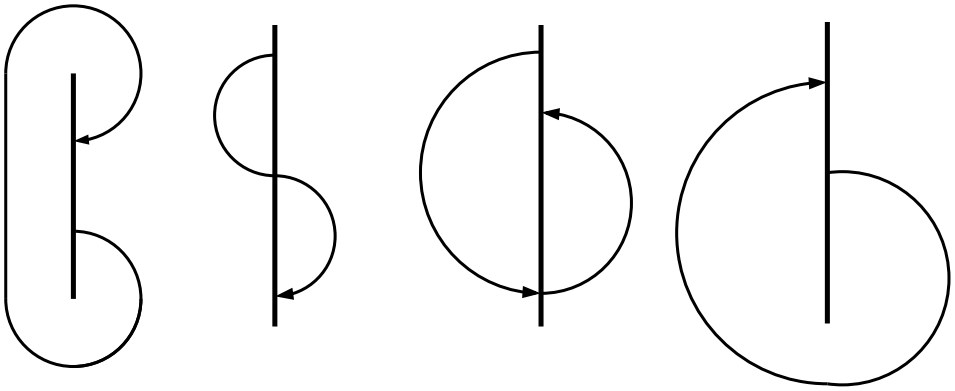

FIGURE 19. A C-curve, S-curve and two types of G-curve. Each is named for the letter it vaguely resembles.

Suppose γ is a returning curve for some N-segment I. A tube consisting of paths parallel to γ is called a return region for I. The tube consisting of all the curves parallel to γ is called a maximal return region for I. Return regions will be named according to the type of curve γ is: C-regions, S-regions and G-regions. Given the returning curve γ, we can construct the corresponding maximal return region in $O(k)$ steps if γ crosses k thin parts. Starting with the first thin part, we simply measure the distance from γ to each end of the thin part along the N-foliation and remember the minimum in each direction (to the left and right of γ). See Figure 20.

We say an E-path has k steps if it crosses k thin parts. We say that it crosses a tube if its intersection with the tube hits every N-segment in the tube.

Lemma 4.2. *Let m be the number of thin parts. There is a collection of $O(n)$ return regions so that any E-path that crosses $> 4m$ thin parts must cross one of these return regions.*

Proof. Each maximal return region contain a boundary point of W on both of its E-sides (otherwise it would not be maximal). Choose one of these and consider the

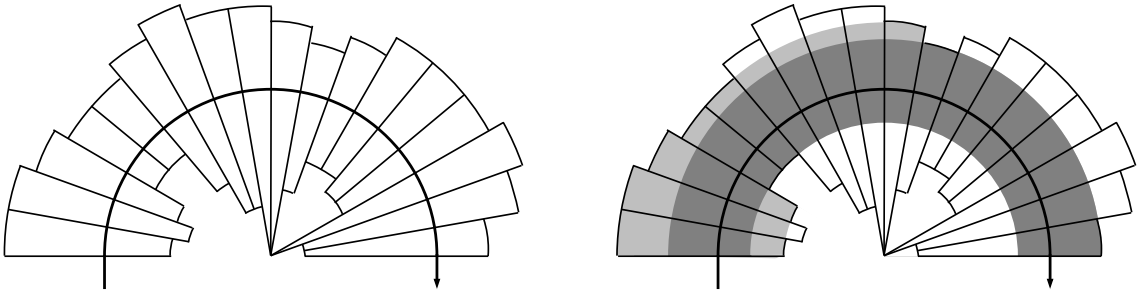

FIGURE 20. Once we have a path that crosses a return region (top picture), we can construct the entire return region in a $O(k)$, if the region uses k thin pieces.

widest return region associated to this point. Since there are only $O(n)$ boundary vertices in W and only one widest return region for each vertex, this defines a collection of $O(n)$ return regions. Fix one of them. Any narrower return region associated to the same vertex has the property that any E-path that crosses it also crosses the wider return region and the two crossing subpaths overlap. Since any path with $2m + 1$ steps (a step refers to crossing a thin part) crosses some return region, any path with $4m + 1$ steps must cross one of our chosen "widest" return regions. □

5. Bending propagation paths

The Gabriel condition gives us a little freedom to change the propagation paths due to the fact that the thin pieces have positive thickness. Consider Figure 21. On the left it shows three propagation paths; suppose we want to shift the middle path without changing the top or bottom path. We can move the righthand vertex on the middle path up or down on the thin edge, as long as it does not enter the shaded disks centered on the other thin edge. Moreover, the new disks formed by moving the point should not contain the middle vertex on the left segment. In this section we estimate how much we can bend an E-path and still have the Gabriel property. This is the main calculation on which the estimate in Theorem 1.1 rests.

We can always subdivide a thin sector of angle θ into k sectors of angle θ/k and increase the number of thin parts by a factor of k. Fix an angle $0 < \theta_0 < 30^\circ$ and assume that we have done this, where necessary, so that all the thin sectors have angle $\leq \theta_0$.

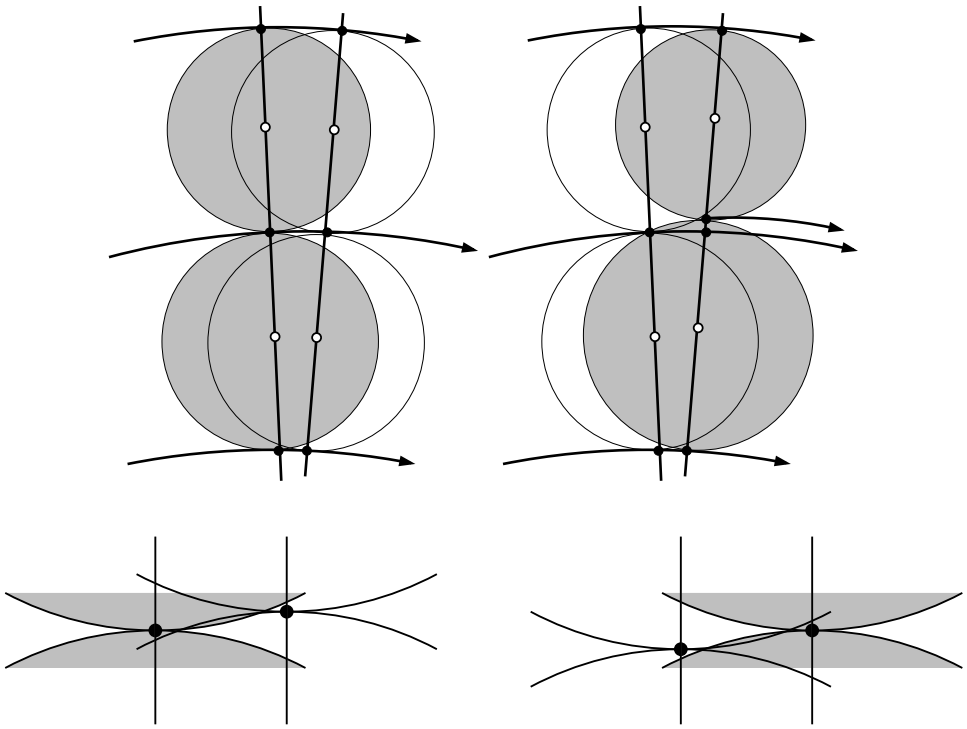

FIGURE 21. We can slightly alter a propagation path and maintain the Gabriel condition. The new point on the right segment has to stay outside the shaded disks on in the left picture and the old point on the left segment must be outside the shaded disks in the right picture. The situation is enlarged in the bottom pictures.

A Gabriel path γ in a tube S is defined to be a path with the following properties. First, γ is a path in S with its initial endpoint on an N-side of the tube. Let V be the set of points where γ crosses an open N-segment. Each N-segment contains at most one point of V and whenever an N-segment I does contain a point $v \in V$ the two components of $I \setminus \{v\}$ are diameters of disks in S that contain no points of V. Each N-segment I that does not intersect V is itself the diameter of a disk not hitting V. See Figure 22.

Clearly any E-path crossing S is a Gabriel path. We want to show that if the tube is long and narrow then any E-path crossing S can be replaced by a Gabriel path with the same starting point but ending somewhere inside S.

Lemma 5.1. *There is a constant $M < \infty$ so that the following holds. Suppose S is a tube of width w, length L and is a union of k sectors. Suppose that $L \geq M\sqrt{k}w$.*

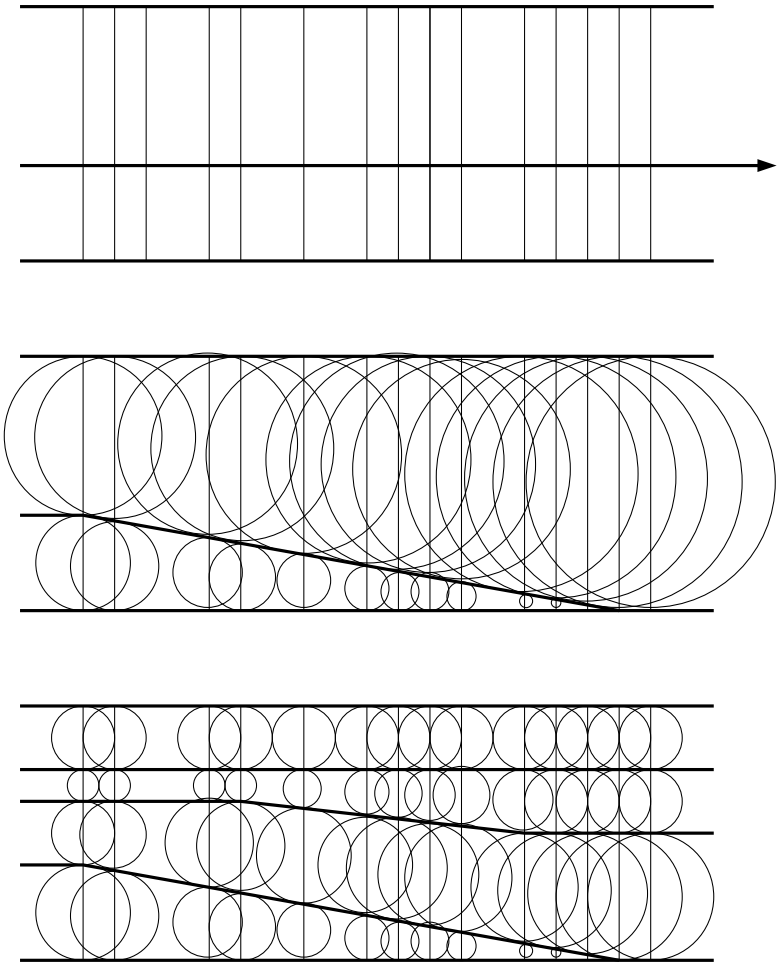

FIGURE 22. Replacing a E-path (top) by a terminating Gabriel path (middle). If we later add more paths to the tube, the disks get smaller and hence the Gabriel condition still holds (bottom).

There is a N-segment I of the tube so that any E-path γ that enters the tube can be replaced by a Gabriel path γ' with the same starting point, but that terminates without crossing I.

If one E-path in a tube can be replaced, then any number of E-paths can be replaced, since further subdivision of the N-segments only makes it easier for the Gabriel condition to hold.

The proof of Lemma 5.1 will proceed in several steps. The first observation is that if the tube contains a "fat" sector then there is nothing to do.

Lemma 5.2. *Let $\eta = (\sin\theta_0)/(\theta_0(1+\sin\theta_0))$. Suppose S is a truncated sector with angle $\theta \le \theta_0$. Suppose the N-sides of S have length w and the longer E-side has length ℓ. If $w \le 2\eta\ell$ then any half-disk with base on one N-side of S does not intersect the other N-side.*

Proof. Consider Figure 23. Let $R = |a-d|$ so that $\ell = R\theta$ and $r = (R-r)\sin\theta$, so

$$r = \frac{R\sin\theta}{1+\sin\theta} = \ell\frac{\sin\theta}{\theta(1+\sin\theta)} \ge \ell\frac{\sin\theta_0}{\theta_0(1+\sin\theta_0)} = \ell\eta.$$

Note that $\eta \to 1$ as $\theta_0 \to 0$. If $w \le 2\eta\ell/$ then $w \le 2r$ and any halfdisk with base on the N-side of the sector can't hit the opposite N-side. □

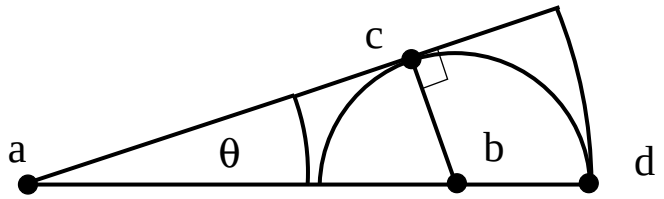

FIGURE 23. If $w \le 2\eta\ell$ then disks centered on an N-side of a sector don't hit the other N-side. Gabriel paths end if they hit such a sector.

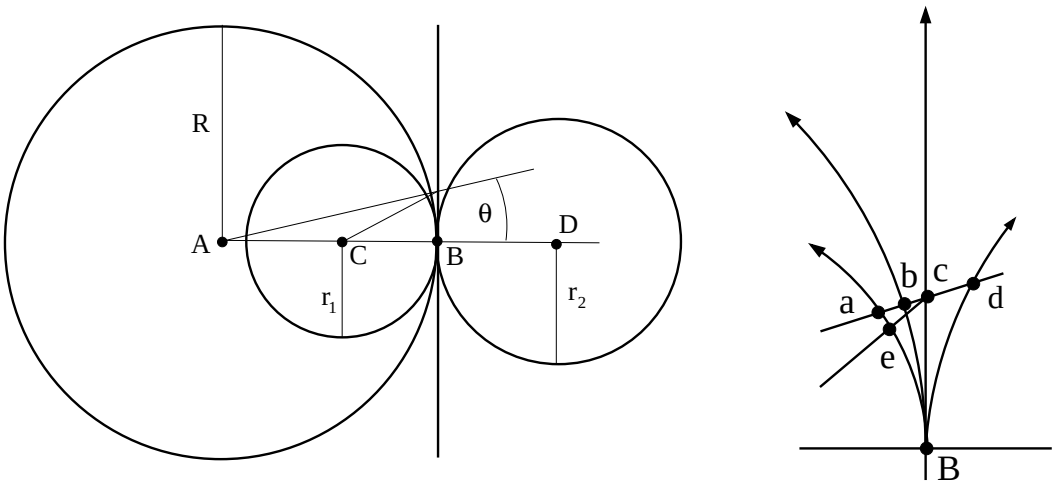

FIGURE 24. The figure illustrates how much we can perturb a Gabriel path.

If a Gabriel path encounters a fat sector then we can terminate the path there. So next we have to bend propagation paths assuming every sector in the tube satisfies $w > 2\eta\ell$. How far can we bend a path in each sector? Consider Figure 24. Suppose S

is a proper sector with vertex A, angle $\theta > 0$ and sides L_1, L_2. Let B, C, D be points on L_1 so that $D_1 = D(C, r_1), D_2 = D(D, r_2)$ be two disjoint disks that are tangent at the point B and neither open disk contains the vertex A. Let $R = |A - B|$. The disk D_1 does not contain A, so $r_1 \leq R/2$. The point a is the point of $\partial D_1 \cap L_2$ farther from A, b is $\partial D(A, R) \cap L_2$, c is where the perpendicular to L_1 through B hits L_2 and d is the point of $\partial D_2 \cap L_2$ closer to A. Let e be the point where the segment $[C, c]$ crosses ∂D_1. Let $x = |c - B|$. Then

$$x = R \tan\theta = \ell \frac{\tan\theta}{\theta} \leq \ell \frac{\tan\theta_0}{\theta_0} = \ell\mu.$$

Since we are assuming $\ell \leq w/(2\eta) = r_1/2$, we $x \leq \mu\ell \leq w\mu/(2\eta) = r_1\mu/\eta$.

By the mean value theorem we have for $x, y > 0$

$$\sqrt{y} + \frac{x}{2\sqrt{y+x}} \leq \sqrt{y+x} \leq \sqrt{y} + \frac{x}{2\sqrt{y}}.$$

Since $\theta \leq 30^\circ$ we have $x \leq \frac{1}{2}R$ and hence

$$|b - c| = \sqrt{R^2 + x^2} - R \geq R + \frac{1}{2}\frac{x^2}{\sqrt{R^2 + x^2}} - R \geq \frac{1}{\sqrt{5}}\frac{x^2}{R} \tag{5.1}$$

and

$$|b - c| = \sqrt{R^2 + x^2} - R \leq R + \frac{1}{2}\frac{x^2}{\sqrt{R^2}} - R \leq \frac{x^2}{2R}.$$

Thus

$$\frac{1}{\sqrt{5}}\frac{x^2}{R} \leq |b - c| \leq \frac{1}{2}\frac{x^2}{R}.$$

Since $[e, c]$ is perpendicular to ∂D_1 we have

$$|a - c| \geq |e - c| \geq \sqrt{r_1^2 + x^2} - r_1 \geq \frac{1}{2}\frac{x^2}{\sqrt{r_1^2 + x^2}} \geq \frac{1}{2\lambda}\frac{x^2}{r_1}.$$

where $\lambda = \sqrt{1 + (\frac{\mu}{\eta})^2}$. We want $\lambda < 2$. A simple calculation shows this happens exactly when

$$\begin{aligned}
\eta^2 + \mu^2 &< 4\eta^2 \\
\mu &< \sqrt{3}\eta \\
\frac{\tan\theta_0}{\theta_0} &< \sqrt{3}\frac{\sin\theta_0}{\theta_0(1 + \sin\theta_0)} \\
1 + \sin\theta_0 &< \sqrt{3}\cos\theta_0 \\
\theta_0 &< 30^\circ,
\end{aligned}$$

which is why we choose θ_0 as we did. Thus

$$|a-b| \;=\; |a-c|-|b-c| \geq \frac{1}{2\lambda}\frac{x^2}{r_1} - \frac{1}{2}\frac{x^2}{R} \geq (\frac{1}{2\lambda}-\frac{1}{4})\frac{x^2}{r_1}$$

so setting $c = (\frac{1}{2\lambda}-\frac{1}{4})$, we have

$$|a-b| \;\geq\; c\frac{x^2}{r_1} \geq c\frac{x^2}{R}.$$

For the other disk, similar calculations to (5.1) give

$$|b-d| \;=\; |b-c|+|c-d| \geq \frac{1}{\sqrt{5}}\frac{x^2}{R} + \frac{1}{\sqrt{5}}\frac{x^2}{r_2} \tag{5.2}$$

if $2r_2 \geq \eta\ell$.

Proof of Lemma 5.1 . Suppose S is a tube of width w and length L (this is the length of the shorter E-side). For the jth sector let ℓ_j be the length of the mid-path of the sector and let L_j be the length of the longer E-side of the sector. Note that $\ell_j \leq L_j$ and $\sum_j \ell_j = L_{1/2} \geq L$ by Lemma 3.1.

If the tube has a fat sector (i.e., $L_j \geq w/2\eta$) then we simply end E-paths when they hit it. Otherwise, there are no fat sectors, so $\ell_j \leq L_j \leq w/(2\eta)$ for every j. Since we may assume $\frac{1}{2} < \eta < 1$, we can deduce that if $L \geq 8w$, then $\ell_j \leq w/(2\eta) \leq \frac{1}{8}L \leq \frac{1}{4}L_{1/2}$. Thus we can split the tube into two tubes joined end-to-end at an N-segment I so that $\sum \ell_j \geq \frac{1}{4}L$, in each sub-tube.

Since there are no fat sectors, the calculations above show that the we can create a Gabriel path by shifting by $c\ell_j^2/w$ in the jth sector. Thus the Cauchy-Schwarz inequality implies that summing over each of these tubes gives

$$\frac{1}{16}L^2 \leq (\sum_j \ell_j)^2 \leq k\sum_j \ell_j^2,$$

where k is the number of sectors in the tube. Thus

$$\sum_j \frac{\ell_j^2}{w} \geq \frac{1}{16}L^2\frac{1}{k}\frac{1}{w} \geq \frac{(M\sqrt{k}w)^2}{16kw} \geq \frac{Mw}{16},$$

so if $M \geq 16/c$, we can make the Gabriel path hit either side of the tube. □

The arguments given above also prove (even more easily) that a propagation line can be bent by at least $c\theta\ell$ if the sector has angle θ.

6. Laying the traps

In this section we lay traps in each return region. Each region has a slightly different form of trap, but each involves placing $\sqrt{n}$ parallel E-paths in the return region to form long narrow tubes and bending each propagation path that enters a tube so that it terminates in the tube. Thus all of the original propagations paths terminate before crossing $O(n)$ thin parts, creating $O(n^2)$ vertices. However, we have created $O(n^{1.5})$ tubes and the endpoints of these tubes are propagated for $O(n)$ steps as well, creating a total of $O(n^{2.5})$ new vertices. We consider each type of return region separately. Recall that the width of a tube is the length of its N-sides and the length of the tube is the length of its shorter E-side.

Lemma 6.1. *The length L of a C-region is at least twice its width w.*

Proof. By definition, the N-sides of a C-region are disjoint intervals on the same N-segment J, so the length of J is at least $2w$. But both E-sides of the region cover J when projected orthogonally onto the line containing J, so $L \geq |J|$. □

By Lemma 5.1 we now get

Corollary 6.2. *Suppose a C-region consists of k sectors. Divide it into $\lceil 2\sqrt{k}M \rceil$ equal width tubes. Then every E-path that enters the region from either side can be bent to hit the side of one of the tubes before it is halfway through the region. This always holds with $k = O(n)$, since there are at most $O(n)$ distinct thin parts.*

This gives the traps for C-regions. Next we turn to S-regions, each of which we split into four sub-tubes as follows. Suppose Y is a S-region of width w. Then Y is associated to two U-regions, U_1, U_2, which meet end-to-end. Each of these are split into two thinner tubes by the central E-path. The longer sub-tube is called the outer part and the shorter is called the inner part. The four resulting regions are denoted $U_1^i, U_1^o, U_2^i, U_0^o$. Note that the inner part of U_1 meets the outer part of U_2 along a common N-segment. See Figure 25. Thus every E-path that enters Y, must enter one of the two outer parts.

Lemma 6.3. *The length of U_j^o, $j = 0, 1$ is at least $\pi w/2$.*

Proof. Each outer part is separated by the corresponding inner part from thin part vertices whose angles sum to at least π. Since the inner part has width $w/2$, the

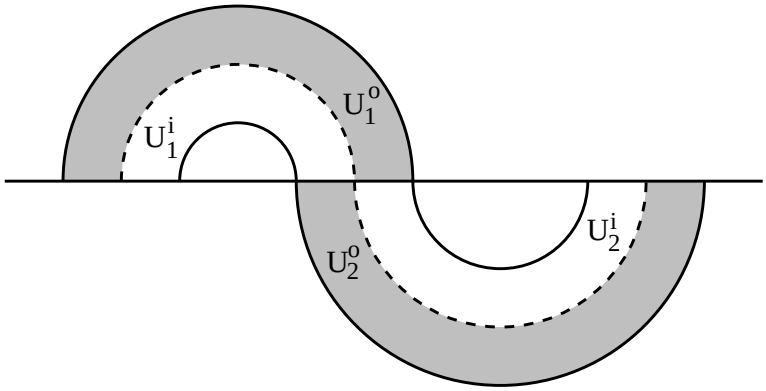

FIGURE 25. The outer regions of a S-region are shaded. These are where we place the traps.

common E-edge of the inner and outer parts has length $\pi w/2$ (by Lemma 3.1) and the other E-edge of the outer part has length at least πw. □

Corollary 6.4. *Suppose Y is a S-region with k sectors. Divide U_1^o and U_2^o into $\lceil M\sqrt{k}\rceil$ equal width tubes. Then every E-path that enters Y can be bent to hit a side of a tube.*

Next we turn to G-regions. This is the most complicated case. A G-region has two ends I, J on the same N-segment. If I and J are disjoint then the region is a tube whose length is at least its width. See the left side of Figure 26. In this case we add $O(\sqrt{n})$ even spaced trapping paths just as for C-regions.

The more interesting case is when I and J overlap, then the G-region is a spiral: we can extend the inner E-boundary as a E-path that spirals in the region until it eventually leaves through J (or hits an endpoint of J). See Figure 26. Any E-path the enters the spiral will enter it across one of the segments $I \setminus J$ or $J \setminus I$ and can be propagated until it leaves through the other one. The number of times the E-path spirals is called the radius R of the spiral (this approximately the ratio of $|I|$ to $|I \setminus J|$) and may be arbitrarily large, independent of n. Thus we must be careful not to let a path spiral all the way through a G-region. A spiral is shown in Figure 18.

If the G-region is a spiral, then construction of the traps is more complicated and breaks into five stages, depending on how large R is:

(1) $R = O(1)$.
(2) $R = O(n^{1/3})$.

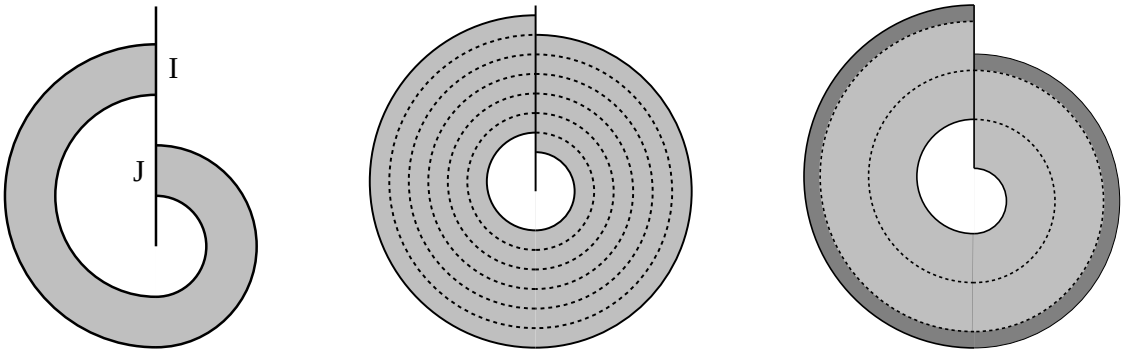

FIGURE 26. A G-region is a union of parallel G-curves. The region can form a single tube with disjoint ends (left) or the two ends can overlap can overlap. In this case, extending the inner boundary creates a spiral in the region. This path may hit the endpoint of the outer E-boundary (center) or may hit the interior of the exit segment (right). By removing a tube from the outermost spiral, we can always reduce the second case to the first case.

(3) $R = O(n^{1/2})$.
(4) $R = O(n)$.
(5) $R \gg n$.

The whole spiral is divided at $R/2$ into an inner and outer part. The construction below is given for the inner part, but is replicated on the outer part (where it is much easier since all the spirals are much longer). For a given value of R we first construct all the previous stages (so each stage adds onto the previous ones). For simplicity we rescale so that the entrance and exit segments have length 1.

Stage 1: If $R = O(1)$, we simply place $O(n^{1/2})$ equally spaced leaves in the spiral and treat the serial like a C-region or S-region. Every path entering the spiral is perturbed to terminate on a trap leaf within 1 turn of the spiral. See Figure 27.

Stage 2: In the next phase we start to merge the remaining $O(n^{1/2})$ trapping leaves. Suppose there are $M = O(n)$ trapping curves in the first spiral and that they are $1/M$ apart. In the next spiral we can merge pairs of adjacent leaves, leaving $M/2$ distinct paths that are now $2/M$ apart. We can merge each of these after two spirals, leaving $2^{-2}M$ paths that are $2^k/M$ apart. In general when we have $2^{-k}M$ parallel leaves distance $2^k M^{-1}$ apart, we can merge pairs of them after 2^k more spirals. At

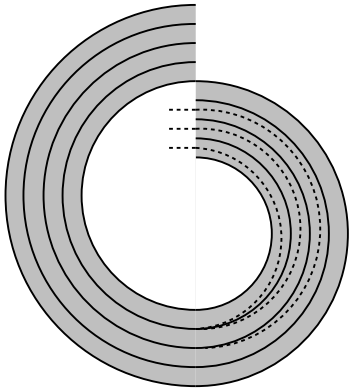

FIGURE 27. In the first spiral we introduce $\sqrt{n}$ trapping paths and bend all entering paths to hit one of these.

each stage the number of vertices generated is most

$$n \times \#\text{spirals} \times \#\text{leaves} = n \cdot 2^k \cdot 2^{-k} M = O(n^{1.5}).$$

The number of stages is $O(\log n^{1/2}) = O(\log n)$. Thus the total number of new vertices is $O(n^{1.5} \log n)$. See Figure 28.

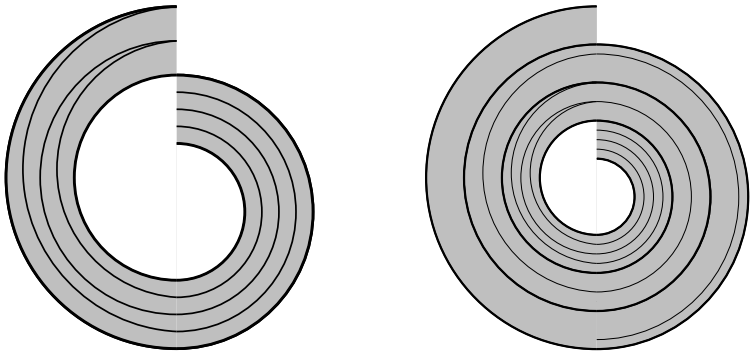

FIGURE 28. In Stage 2, we bend the trapping paths towards each other. After one spiral we cut the number in half. After two more spirals we remove half of the remaining ones. Clearly we can reduce the number by a factor of 2^{-k} after 2^k spirals, but because the spirals get longer as we move out, we can actually do better, as described in the text.

This is a little bigger than we want, but we can get rid of the $\log n$ by being more careful. The argument above assumes it takes 2^k spirals to merge leaves that are $\simeq 2^k n^{1/2}$ apart. This is correct if each spiral has the same length, but the farther out

we go, the longer the spirals become (the jth spiral has length $\simeq j$), so fewer spirals are needed to merge the paths.

Let $\lambda = 2^{2/3}$. Suppose at the radius $\sim \lambda^k$ we have $2^{-k}M$ paths, about distance $2^k/M$ apart. The tube that spirals from radius λ^k to λ^{k+1} crosses $O(\lambda^k n)$ thin parts, and has length comparable to

$$\sum_{j=\lambda^k}^{\lambda^{k+1}} j \quad \sim \quad \lambda^{2k}.$$

Therefore, by Lemma 5.1, we can merge adjacent paths if

$$\lambda^{2k} \gg C\sqrt{\lambda^k n}2^k/M.$$

Since $M \sim \sqrt{n}$, we need $\lambda^{2k} \gg \lambda^{k/2}2^k$, which implies we want $\lambda > 2^{2/3}$. Thus the total number of new vertices is

$$n \sum_{k=1}^{\lceil \frac{1}{2}\log_2 n\rceil} 2^{-k}M\lambda^k = O(n^{1.5}) \sum_{k=1}^{\infty} 2^{-k}2^{\frac{2}{3}k} = O(n^{1.5}).$$

Moreover, the total number of spirals used is

$$\sum_{k-1}^{\lceil \frac{1}{2}\log_2 n\rceil)} \lambda^k = O(\lambda^{\frac{1}{2}\log_2 n}) = O(2^{\frac{2}{3}\frac{1}{2}\log_2 n}) = O(n^{1/3}).$$

Thus when we reach radius $n^{1/3}$ we have merged the original M trapping paths into a single path.

Stage 3: The third phase is easy: just take the single path created in the last stage and propagate it from $n^{1/3}$ to $n^{1/2}$ along the E-foliation. This introduces $O(n^{1.5})$ new vertices. See Figure 29.

Stage 4: At radius $n^{1/2}$ we can finally perturb the propagation curve to hit itself, assuming we put another closed propagation curve at most distance 1 further out. We now form closed loops along a sequence of radii $\{r_k\}$. The annular regions between the closed loops have width $w \simeq r_{k+1} - r_k$, so our estimates in Section 5 say we can do this if $r_{k+1} - r_k = w \simeq {r_k}^2/n$. Suppose $r_k = n^{\beta_k}$. Then this estimate becomes $n^{\beta_{k+1}} - n^{\beta_k} \simeq n^{2\beta_k - 1}$, which is the same as,

$$n^{\beta_{k+1}} = n^{\beta_k} + O(n^{2\beta_k - 1}) = n^{\beta_k}(1 + O(n^{\beta_k - 1})),$$

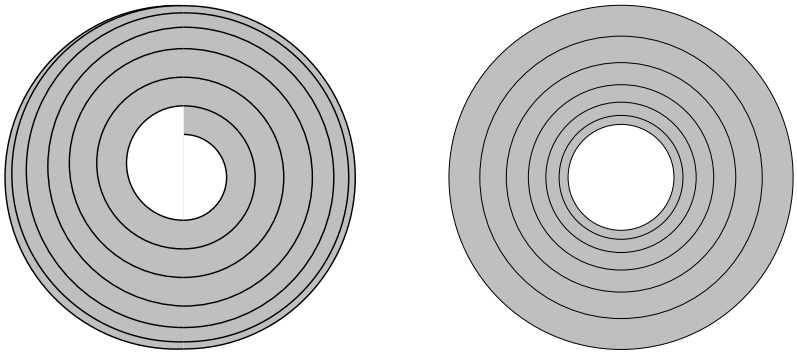

FIGURE 29. In Stage 3 (left), we let a single curve spiral around $O(\sqrt{n})$ times, after which it can be bent to hit itself. In Stage 4 (right) we fill the region with closed paths. Spacing between the closed loops is ~ 1 near radius $\sqrt{n}$ and grows to $\sim n$ near radius n.

or taking logs and dividing,

$$\beta_{k+1} = \beta_k + O(\frac{n^{\beta_k - 1}}{\log n}). \tag{6.1}$$

Since $\beta_k \geq \frac{1}{2}$, this is satisfied if we take steps of size $\beta_{k+1} - \beta_k = O(\frac{n^{-1/2}}{\log n})$, and this implies we reach $\beta_k = 1$ after $O(n^{1/2} \log n)$ steps. Thus $O(n^{1/2} \log n)$ closed curves are placed between spirals $\sqrt{n}$ and n, creating a total of $O(n^{1.5} \log n)$ vertices. As before, we have to work a little harder to get rid of the $\log n$ term.

We want β_k to increase from $\frac{1}{2}$ to 1 in only $\sqrt{n}$ steps, while satisfying (6.1). To do this we divide the interval $[\frac{1}{2}, 1]$ into $m = \log_2 n$ subintervals of the form $I_j = [\frac{1}{2} + 2^{-j}, \frac{1}{2} + 2^{-j+1}]$, for $j = 2, 3, \ldots m$ (without loss of generality we can assume $n = 2^m$ is a power of 2). We let $\beta_0 = \frac{1}{2}$ and $\beta_1 = \frac{1}{2} + \frac{n^{-1/2}}{\log n}$. In general, if β_k is in I_j we define $\beta_{k+1} = \beta_k + \frac{n^{-\frac{1}{2}+2^{-j}}}{\log n}$. It then takes $2^{-j} n^{\frac{1}{2}-2^{-j}} \log n$ steps for β_k to "march across" I_j. Let $M = \lfloor \log_2 m \rfloor - 4$. The total number of steps needed for β_k to increase from $\frac{1}{2}$ to 1 is

$$\begin{aligned}
\sum_{j=2}^{m} 2^{-j} n^{\frac{1}{2}-2^{-j}} \log n &= \sqrt{n} \log n \sum_{j=2}^{m} 2^{-j} 2^{-m2^{-j}} \\
&= \sqrt{n} \log n (\sum_{j=2}^{M} 2^{-j} 2^{-m2^{-j}} + \sum_{j=M+1}^{m} 2^{-j} 2^{-m2^{-j}}) \\
&= \sqrt{n} \log n (I + II),
\end{aligned}$$

where I and II denote the two sums. To handle sum II we simply use $2^{-m2^{-j}} \leq 1$ to get

$$II \leq \sum_{j=M+1}^{m} 2^{-j} = O(2^{-M}) = O(\frac{1}{\log n}).$$

To estimate sum I, we use the ratio test from calculus: the ratio of the $(j-1)$st term divided by the jth term is

$$\frac{2^{-j+1-m2^{-j+1}}}{2^{-j-m2^{-j}}} = 2^{1-m(2^{-j+1}-2^{-j})} = 2^{1-m2^{-j}} \leq 2^{1-2^4} \ll \frac{1}{2}$$

where the final inequality holds since $j \leq M$ in the sum, so $2^{-j} \geq 2^{-M} \geq 2^{-\log_2 m-4} \geq \frac{1}{m}2^4$. Thus the series is geometrically increasing and is dominated by a multiple of its last term $j = M$. This gives

$$\sum_{j=2}^{\log m} 2^{-j-m2^{-j}} = O(2^{-M-m2^{-M}}) = O(\frac{1}{m}) = O(\frac{1}{\log n}).$$

Thus $\sqrt{n}\log n(I + II) = O(\sqrt{n})$, which is the desired estimate: only $O(\sqrt{n})$ closed loops are needed to fill the region between radii $\sqrt{n}$ and n.

Stage 5: Once we reach $R \simeq n$, we can take the width of the outer tube to be ∞ and still perturb to a closed curve by (5.2). Thus no further vertices need be added beyond this. The spiral is empty until we come within $O(n)$ of the outer boundary and reach the innermost closed path constructed starting from the outer edge of the spiral.

The construction above is given starting from the inner boundary and working outward. A similar construction is possible starting at the outermost spiral and working inward, but is easier since each spiral is longer than the corresponding one in the inner part of the G-region. Near the center of the spiral, the two constructions have to joined. The details of this depend on which stage the construction is in, but is easy in every case.

7. Proof of Theorem 1.1

We can now complete the proof of Theorem 1.1. Given a PSLG we triangulate it and let Γ be the resulting PSLG. For each triangle, compute the thick and thin parts. Find the $O(n)$ maximal return regions and construct the $O(\sqrt{n})$ traps per region. Take the collection of all vertices on the N-sides of the thin region together

with the trapping vertices, i.e., the endpoints of all traps. This is $O(n^{1.5})$ points and each point has a associated direction along the E-foliation (into the thin part for boundary vertices and away from the trapping edge for the return region vertices). For each point, follow E-foliation until it either hits the boundary of W or enters a return region by crossing an N-side of the that region (because return regions may overlap, a trapping vertex may start in the interior of a return region, but we wait until the E-path starting there enters a new region through its N-side). This takes at most $O(n)$ steps for one of these alternatives to happen (a step is crossing one thin part). If the E-path hits the boundary we stop and declare the path we created to be fixed.

Otherwise, the path enters a return region. When the path enters a tube of a return region we being bending it towards a side the tube (to be concrete, we bend to the right with respect to the path's direction). Continue until the path hits a fixed path and then stop. This may either be the side of the tube, or an E-path that was created earlier. Since we know we will hit the side of the tube before crossing all the way through the return region, the path must stop within $O(n)$ steps. The stopped path is then declared to be fixed.

Every vertex is thus propagated and stopped after at most $O(n)$ steps, creating at most $O(n^{2.5})$ new vertices. The intersections of these paths with the sides of the thin parts define Gabriel edges by the construction of each path (and the addition of more paths later in the construction does not change this). Thus we can acutely triangulate each triangle using the argument of Section 2. This proves Theorem 1.1.

8. β-skeletons and almost nonobtuse triangulation

Suppose we are given a finite point set V. Recall that a segment $S = [v, w]$, $v, w \in V$ is called a Gabriel edge if the open disk with diameter S contains no point of V. This is an example of an "empty region" graph on V, i.e., a graph where a segment $S = [v, w]$ is included iff some region associated to S contains no points of V.

Another such example is the β-skeleton. For $\beta \in [0, 1]$ the region associated to $S = [v, w]$ is the set of points from which S subtends angle $\theta = \pi - \arcsin(1/\beta)$. Note that for β close to 1, we have $\theta \simeq \sqrt{1 - \beta}$. This region is the intersection of two disks

of radius $|v-w|\beta$ that both have S as a chord. See Figure 30. For $\beta = 1$, this is the same as the Gabriel disk, so the 1-skeleton is the same as the Gabriel graph. For $\beta \leq 1$, the β-skeleton contains the Gabriel graph, so every PSLG has a conforming β-skeleton of size $O(n^{2.5})$. In fact, we can improve this to $O(n^2/(1-\beta))$ (Theorem 1.9).

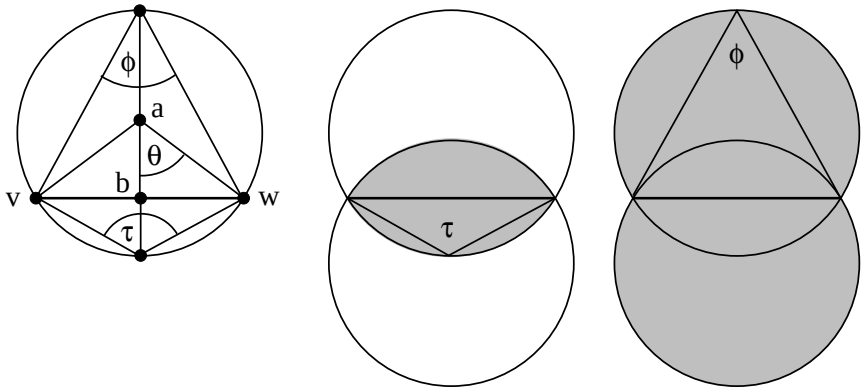

FIGURE 30. Suppose $|v-w| = 1$ and $|a-w| = \alpha/2$. Then $\theta = \arcsin\frac{1}{\alpha}$, so $\phi = 2(\frac{1}{2}(\pi - (\pi - \theta)) = \theta$ and $\tau = \pi - \phi$. If $\alpha = \beta < 1$ this shows the empty region for the β-region is an intersection of disks of radius $\beta|v-w|$ and also the set of points for which $[v,w]$ subtends angle less than $\tau = \pi - \arcsin\beta$. If $\alpha = \frac{1}{\beta}$, this shows the circle based β-region is a union of disks of diameter $\beta|v-w|$.

The proof is roughly the same as for Theorem 1.1, except that we now have more freedom to bend the E-paths (and hence can stop them sooner). Suppose we fix an angle $\theta > 0$. First divide every thin piece into pieces of angle $\leq \theta/2$. Each thin part is divided into at most $2\pi/\theta$ new pieces, so so the total number of thin pieces increases from $O(n)$ to $O(n/\theta)$. A θ-segment is a line segment with endpoints on distinct N-sides of a thin piece and making angle between $90^\circ - \theta$ and $90^\circ + \theta$ with both sides. Because we have made each thin part have angle $\leq \theta/2$, if γ is an arc of the E-foliation crossing a thin part, then the line segment with the same endpoints is a $\theta/4$-segment. A θ-path is a connected path composed θ-segments chosen so that it does not cross the same thin part on adjacent segment (no sharp turns).

Lemma 8.1. *Suppose γ is an E-path crossing a thin part, with endpoints x, y. Suppose the angle of thin part is $\phi \leq \theta/2$. A θ-segment can connect x to every point of an interval on the N-foliation centered at y and having length at least $c\theta\ell(\gamma)$.*

Proof. Consider Figure 31. This shows a θ-segment $S = [a, c]$ crossing a thin part with angle $\phi \le \theta/2$. Thus S is the base of a isosceles triangle and with base angles $\frac{\pi}{2} - \frac{\phi}{2}$. Let $\tau \le \theta/2$. Also shown are two segments $[a, b]$ and $[a, c]$ that make angle τ with S. Thus both of these make angle $\le \theta$ with both sides of the thin pieces, so are θ segments. By the law of sines

$$\frac{|b-c|}{\sin\tau} = \frac{|a-c|}{\sin(\pi-\alpha-\tau)}$$

so

$$|b-c| = |a-c|\frac{\sin\tau}{\sin(\pi-\alpha-\tau)} \ge |a-c|\frac{2}{\pi}\tau.$$

Similarly

$$|c-e| \ge |a-c|\frac{2}{\pi}\tau.$$

This proves the lemma. □

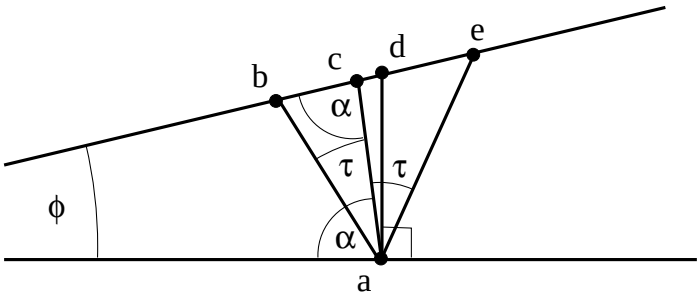

FIGURE 31. Definitions for Lemma 8.1. We assume $\phi \le \theta/2$ and $\tau \le \theta/2$. This implies $[a, b]$ and $[a, e]$ are θ segments.

Thus at each vertex the point that can be reached by a θ path from that vertex form a cone (see Figure 32) which intersects the next N-segment in a "large" interval (depending on θ). If this interval contains a vertex we end the path; otherwise we move it closer to trapping path.

How many vertices are created if we bend θ-paths until they terminate in a trap? We can create traps in our C-regions and S-regions that use $O(1/\theta)$ trapping paths per return region. Since there are $O(n)$ return regions and $O(n/\theta)$ thin pieces, this means that at most $O(n^2/\theta^2)$ vertices are created. For the G-regions, we have to recreate the spiral construction, but there are only three critical radii now instead of five:

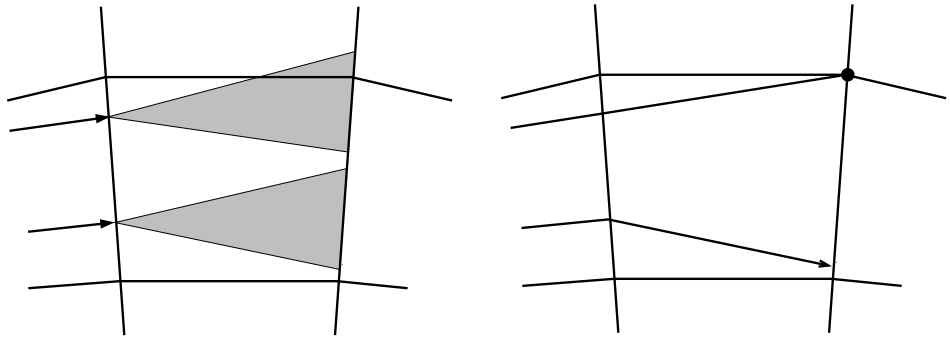

FIGURE 32. Inside a tube, we bend the E-paths to become θ-paths that either hit a vertex (where a fixed path meets a N-side of a thin part) or meets the next N-side closer to the side of the tube by a fixed amount. Every path entering the tube can be bent so its hits the side of the tube; other fixed paths only make it stop sooner. This every path stops before leaving the far side of the tube.

(1) $R = O(1)$.
(2) $R = O(\frac{1}{\sqrt{\theta}})$.
(3) $R = O(\frac{1}{\theta})$.

In the first stage we place $O(\frac{1}{\theta})$ parallel trapping paths and bend all entering propagation paths to hit them. In second stage we propagate the endpoints of the trapping paths. It takes $2^{k/2}$ turns of the spiral to bring together two paths that start distance $2^k\theta$ apart. Thus after $O(\theta^{-1/2})$ spirals we have collapsed all the paths into a single path and created

$$\frac{n}{\theta}\sum_{k=1}^{|\log_2\theta|} 2^{k/2}2^{-k}\theta^{-1} = O(\frac{n}{\theta^2}),$$

new vertices. In the third stage we spiral this path out to radius $\simeq \frac{1}{\theta}$, at which point it can close on itself. This creates $O(\frac{n}{\theta^2})$ new vertices. Once the path can hits itself, no more vertices are needed (unlike the Gabriel case that required a further stage of closed loops). Adding all these contributions gives $O(n/\theta^2)$ per G-region and there are $O(n)$ such regions.

We already know the thick parts can be nonobtusely triangulated with $O(n)$ triangles and if we take the θ-paths created above together with the straight sides of the thin pieces, we break the thin region into $O(n^2)$ triangles and quadrilaterals with no

angles bigger than $90^\circ + \theta$. Adding diagonals to the quadrilaterals proves Theorem 1.4.

If we have a collection of θ-paths crossing the thin region W, we claim the points where they cross the N-sides of thin pieces cut these sides into segments that are in the β-skeleton if $\theta \leq \frac{\pi}{2} - \arcsin(\beta)$. See Figure 33 where we have drawn the side of the thin piece as a horizontal line and the part of the empty region above it is a crescent. By definition of θ, the empty crescent makes an angle $\frac{\pi}{2} - \theta$ with the horizontal and so the empty region lies below the lines starting at the vertices of the crescent and making angle θ with the vertical. If the crescent lies inside the thin part we are done. Otherwise it crosses the far side of the thin part, forming a new crescent above that line. Now however, it makes a smaller angle $\alpha < \frac{\pi}{2} - \theta$ with the side, and hence lies under the lines making angle θ with the lines perpendicular to the new thin side. Thus it also lies below the θ-path started from the first side (the thicker line in the figure). Continuing by induction shows the whole empty region lies between the θ-paths. Since $\theta \simeq \sqrt{1-\beta}$, this proves Theorem 1.9.

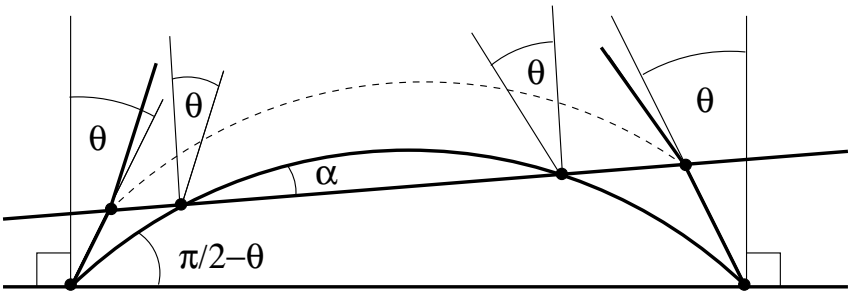

FIGURE 33. The proof that the empty region lies between two θ-path. By definition, the empty region lies between the θ-paths passing through its vertices in the adjacent thin piece. In successive thin pieces, the empty region defines a crescent with even smaller angle, so the argument still works.

We have already shown in Section A that for circle based β-skeletons and $\beta > 1$, there is no bound, depending only on n, for the number of new vertices needed to create a conforming β-skeleton. There is a an alternate definition of β-skeleton in the literature for which such a bound is possible. For $\beta > 1$, a crescent based empty region is the intersection of two disks of diameter $\beta|v - w|$ centered at points that lie on the line through v, w and are distance $\beta = \frac{1}{2}$ from the center of $[v, w]$. Clearly

any Gabriel edge for Γ can be cut into $O(\beta)$ subsegments whose β-crescents lie inside the Gabriel disk. See Figure 34. Thus any PSLG has a conforming crescent based β-skeleton with $O(n^{2.5}\beta)$ vertices.

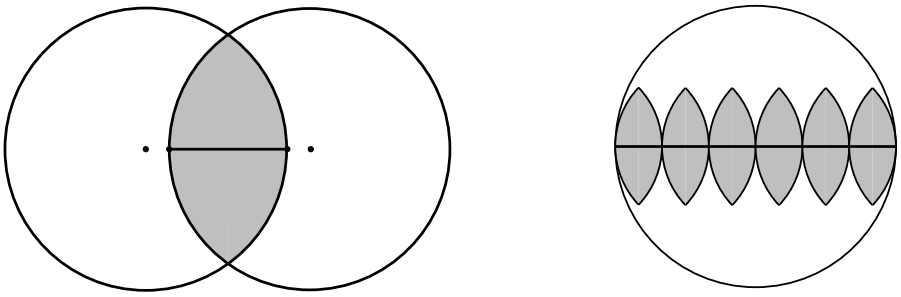

FIGURE 34. The crescent based β-skeleton for $\beta > 1$ uses an empty region for the edge $[v, w]$ that is the intersection of two disks. Clearly any Gabriel edge for Γ can be cut into $O(\beta)$ subsegments whose β-crescents lie inside the Gabriel disk.

9. Connecting components with no small angles

In Section 3 we converted an arbitrary PSLG into a connected PSLG by triangulating it. As noted there, this can introduce small angles. This was acceptable in the proof of Theorem 1.1, but in Theorem 1.5 we want a lower bound on angles, so triangulating the PSLG may not work. In order to connect components of Γ without introducing small angles, we will use a result of David Eppstein [26]: given a PSLG of size n we can add $O(n)$ disjoint open disks (also disjoint from Γ) so that the union of Γ and the boundaries of these disks is a connected set. The disks can be computed in time $O(n \log n)$ (Theorem 1, [26]). We combine this with a simple lemma:

Lemma 9.1. *Given n points on a circle, we can construct a closed simple polygonal curve γ in the corresponding disk that connects the points and has at most $6 + 2n$ sides, has no angles less than 60° and makes no angles smaller than 60° with any segment outside the circle.*

Proof. Assume the disk is the unit disk centered at the origin. For any point x on the boundary of the disk let S_x be the convex hull of x and the disk of radius $\frac{1}{2}$ centered at the origin. This is called a Stolz cone and its boundary consists of two straight segments meeting at x and a portion of the circle of radius 1/2. See Figure 35. Let

S be the union of the Stolz cones over the given set. At each point on the circle, the two edges of the Stolz cone make angle 60° with each other and angle 60° with the tangent to the circle, and hence angle $\geq 60^\circ$ with any segment outside the disk. If the straight segments of the Stolz cones of two adjacent points meet, the angle they form is is $60^\circ + \phi$ where ϕ is the angular separation of the points on the unit circle, hence is between 60° and 180°. If the straight segments for two adjacent points do not meet, then ∂S contains a piece of circular arc and we replace this by a polygonal arc, so that all angles formed are between 60° and 300°; clearly only 6 points need be added in the worst case, which gives the lemma. □

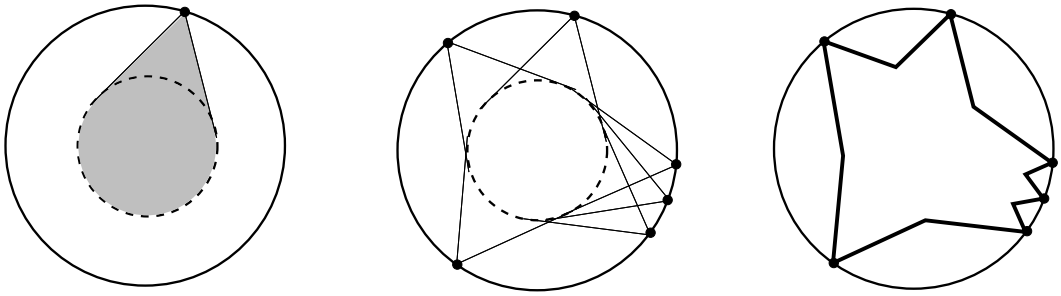

FIGURE 35. On the left is a Stolz cone. A set of n points on a circle can be connected by the boundary of a union of Stolz cones. Any angles formed are $\geq 60^\circ$ (even with segments outside the disk).

Combining the lemma and Eppstein's disk result we have

Lemma 9.2. *Given a PSLG Γ with n vertices, then in time $O(n \log n)$ we can construct a connected PSLG of size $O(n)$ containing Γ and so that any angles $\leq 60^\circ$ were already in Γ.*

Assume that we have replaced Γ by a new PSLG (also called Γ) that has $O(n)$ vertices and that is connected and such that the bounded components of $\mathbb{R}^2 \setminus \Gamma$ are bounded by polygons. Suppose $\{\Omega_j\}$ is a listing of these simply connected components.

Lemma 9.3. *If $\partial\Omega_j$ has n_j vertices, then $\sum_j n_j \leq 6n - 6$.*

Proof. Since each Ω_j is simply connected, n_j is also the number of edges on $\partial\Omega_j$ (counted with multiplicity 2 if Ω_j is on both sides of an edge) and each edge of Γ

can occur in at most two of the Ω_j's. Thus $\sum n_j \leq 2|E|$. Since Γ is a planar graph, $|E| \leq 3|V| - 3$. The result follows. □

10. The thick/thin decomposition for simply connected domains

From the last section we have a PSLG (also denoted Γ) whose bounded complementary components are simply connected polygonal domains. Thus we must extend the idea of the thick/thin decomposition of triangles to simply connected domains. Fortunately, this has already been done in [13]. A crosscut of Ω is a Jordan arc in Ω with both endpoints on $\partial\Omega$. Also recall that the term "sector" can refer to either a proper sector or a truncated sector.

Lemma 10.1. *Suppose Ω is a simply connected, bounded planar domain with a polygonal boundary and n vertices. We can find a collection of $O(n)$ disjoint crosscuts $\{\gamma_j\}$ of Ω that divide Ω into into $O(n)$ subdomains called thick and thin regions. Each crosscut is either a circular arc, a line segment or a union of two circular arcs that have the same tangent direction where they meet. All crosscuts meet $\partial\Omega$ at non-vertex points, and they are perpendicular to $\partial\Omega$ at their endpoints. The hyperbolic distance in Ω between crosscuts is bounded uniformly away from zero and this bound may be as large as we wish (at the cost of increasing the value of M below). Each thin region is either a single sector with two straight sides that are subsegments of sides of Ω or a union of two sectors that share a common straight edge and whose other straight edges are on $\partial\Omega$. Each thick part S is a simply connected subregion bounded by subsegments of $\partial\Omega$ alternating with crosscuts as described above. Each component of $\partial S \cap \partial\Omega$ is a segment that can be broken into subsegments each of which is the base of a half-disk in S. There is constant $M < \infty$, independent of n and Ω, so that if S has k sides, then the total number of these half-disks is $\leq Mk$ and they are all disjoint.*

So we now have a connected Γ and all the bounded complementary components of Γ are decomposed into thick and thin pieces as in Lemma 10.1. The thin pieces divide into two categories: proper sectors and truncated sectors (these categories are called as parabolic and hyperbolic thin parts in [13] and [14] due to an analogy with thin parts in hyperbolic manifolds). The thin region W for Γ will be the union of all truncated sectors (the hyperbolic thin parts). The thick part will be the union of the

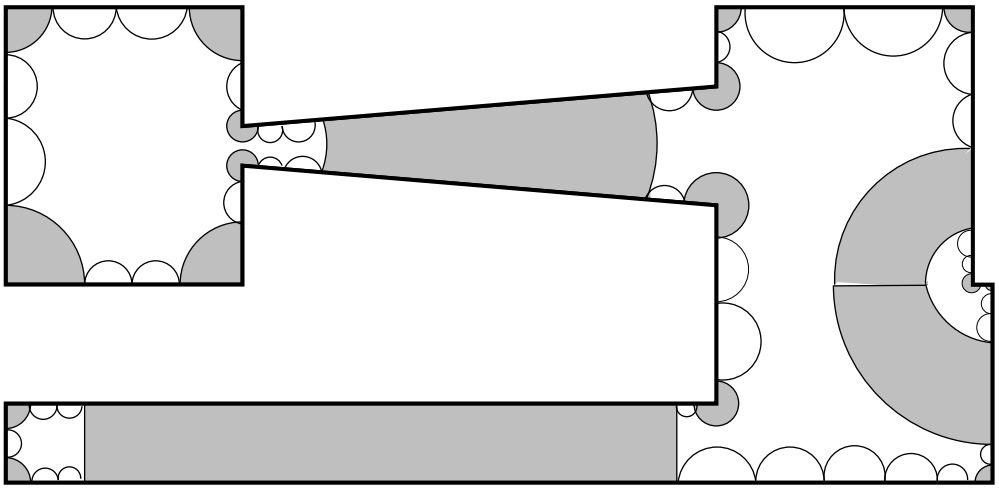

FIGURE 36. The thick/thin decomposition of a polygon. There are three hyperbolic thin parts and 16 parabolic thin parts (this is a cartoon; the thin parts are not drawn to the correct scale).

individual thick parts and the proper sectors (the parabolic thin parts). See Figures 36 and 37.

One slightly annoying feature of the thick and thin parts defined above is that they have a combination of straight edges and circular edges. The edges that lie on the original polygon are, of course, straight line segments. The edges that are crosscuts of the domain are generally circular arcs (although they may be straight if they bound a certain kind of hyperbolic thin part). Because of the curves, we can't hope to mesh these regions with quadrilaterals that only have straight sides. To avoid the problem we introduce "inscribed" thick and thin parts. These simply replace each circular arc crosscut γ by a polygonal crosscut γ' with the same endpoints and whose other vertices are contained in γ. To be precise, we will choose a small angle $\theta_0 > 0$ and subdivide each thin part into sectors of angle $\leq \theta_0$. Thus each thin part is replaced by $O(1)$ thin parts of small angle. The polygonal crosscut is defined by taking the vertices of the new thin parts that lie on a single crosscut.

The polygonal crosscuts subdivide our region into polygonal subregions that have an obvious 1-1 relation to the thin parts and thick parts defined above. We call these the inscribed thick and thin parts. Note that for the thin parts, each proper sector is

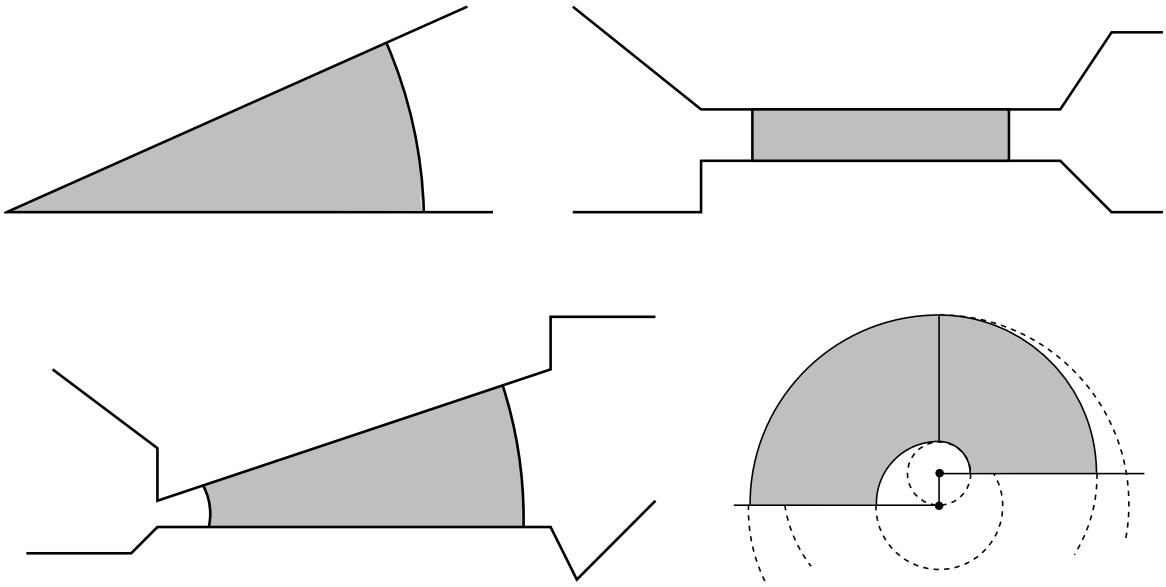

FIGURE 37. Four types of thin parts. The top left is a parabolic thin part and the other three are hyperbolic thin parts. In the final case, we think of the thin part as two thin parts, each a truncated sector with a different center, but sharing a straight edge.

replaced by an isosceles triangle and each truncated sector is replaced by a symmetric trapezoid. In both cases, the angle of the inscribed thin part is the same as the angle of the original thin part. Since they are polygonal, we can attempt to find meshes for them and, in fact, each class has a good quadrilateral mesh. The following lemmas follow from the results in [14]. The first deals with the thick parts.

Lemma 10.2. *Each inscribed thick part S with k sides has an associated quadrilateral mesh with $\leq Mk$ elements and all angles between 60° and 120°. The eccentricity of each piece (the ratio of longest side to shortest side) is uniformly bounded independent of n and S.*

The next deals with thin parts. The inscribed thin parts that are trapezoids are already quadrilaterals, so we only have to describe how to find a quadrilateral mesh for the triangular thin parts.

Lemma 10.3. *Each inscribed thin part that is an isosceles triangle has a quadrilateral mesh with $O(1)$ elements and all angles between 60° and 120°, except that the angle of size θ at the vertex remains if $\theta \leq 60^\circ$. The eccentricity of each piece is*

uniformly bounded, unless $\theta < 60^\circ$ in which case the quadrilateral that contains the vertex of the sector is a kite where the sides opposite the vertex have length that is $\sin(\theta)/(\sqrt{3}\cos(\theta/2)) \sim \theta$ times the length of the sides adjacent to the vertex.

11. Propagation through quadrilateral meshes

Quadrilateral meshes have some convenient properties due to the fact that quadrilaterals have "opposite sides". In this section we review a few of these properties.

Lemma 11.1. *If Ω is a simply connected Jordan region that has a quadrilateral mesh, then the number of mesh vertices on $\partial\Omega$ is even.*

Proof. This is a simple calculation with Euler's formula. Let Q be the number of quadrilaterals in the mesh, I the number of interior vertices, B the number of boundary vertices and E the number of edges. Note the number of edges on the boundary equals B. Each quadrilateral has four edges, and each interior edge is counted twice, so

$$4Q = 2(E - B) + B = 2E - B.$$

By Euler's formula we have

$$1 = (I + B) - E + Q = I + B + \frac{1}{2}(4Q + B) + Q = I + B + \frac{1}{2}B + 3Q.$$

Since all the letters represent integers, $\frac{1}{2}B$ must be an integer too, so B is even. □

Given a quadrilateral with vertices a, b, c, d and a point $x = ta + (1-t)b$ on the edge $[a, b]$, use a line segment to connect x to $y = td + (1-t)c$ on the opposite edge of the quadrilateral. We will call this a propagation line. Replacing x by y and continuing be induction we create a path that continues until we hit a boundary edge (no quadrilateral on the other side) or reach the original starting point x again (if x is a boundary point, this is impossible, so the path must terminate at a distinct boundary point).

Lemma 11.2. *Suppose Q is a quadrilateral with all angles in $I = [90^\circ - \epsilon, 90^\circ + \epsilon]$ that is divided in two by a propagation line L. Each of the resulting subquadrilaterals have angles in I as well.*

Proof. Consider the family of propagation lines L_t, $0 \le t \le 1$ containing L and the angle $\theta(t)$ these lines make with an edge of Q. See Figure 38. We claim this in monotone in t. If not, there are $0 \le t_1 < t_2 < t_3 \le 1$ where $\theta(t_1) = \theta(t_3)$. Suppose the corresponding lines are L_1, L_2, L_3 and let E_1, E_2 be the subsegments of ∂Q that connect the endpoints of L_1 and L_3. Then L_1 and L_3 are parallel and since the endpoints of L_t move linearly with t, L_1 must also be parallel to both of them, so $\theta(t_2) = \theta(t_1)$. This implies α is monotone. □

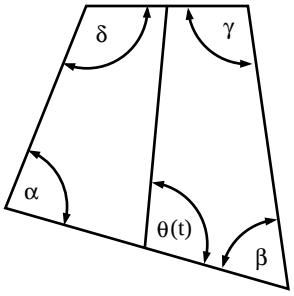

FIGURE 38. Labeling of the angles in the proof of Lemma 11.2.

A refinement of a mesh is another mesh obtained by subdividing some (or all) of the quadrilaterals. A mesh produced by adding a finite number of propagation paths will be called a simple refinement.

Lemma 11.3. *Suppose Ω is polygonal domain and every component of $\partial\Omega$ is a closed Jordan curve. Then any quadrilateral mesh of Ω has a simple refinement with exactly twice as many vertices on each component of $\partial\Omega$.*

Proof. Just split each quadrilateral into four by two segments joining the midpoints of opposite sides. Each boundary edge is split in two so the number of boundary edges on each component doubles. Alternatively, one can just split each boundary edge into two, and propagate these vertices until the hit another boundary midpoint. See Figure 39 □

12. The proof of Theorem 1.5

In this section we prove Theorem 1.5 except for except for the construction of certain special meshes called sinks; these are described in the next section.

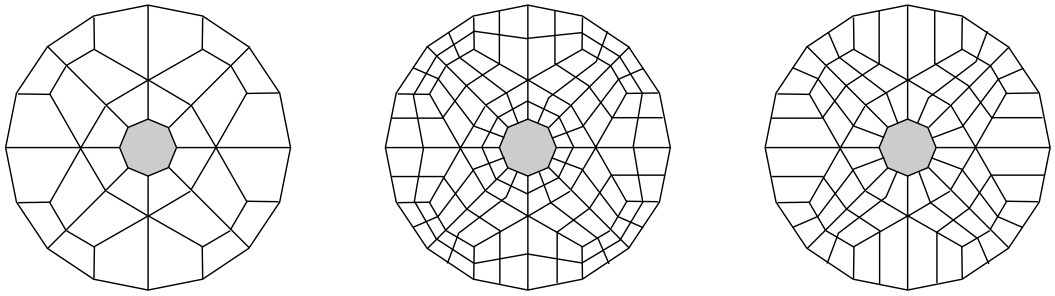

FIGURE 39. A mesh of an annular region (left) and its double (center). On the right we only double the boundary edges and propagate these.

The general idea for proving Theorem 1.5 is similar to what we did for Theorems 1.1 and 1.4. Associated to Γ there will be a thin region W and a collection of thick pieces. We find a mesh on each thick piece; this gives a collection of vertices on the boundary of the thin region. Each of these vertices is propagated across the thin region by following the E-foliation as before. Also as before we bend the propagation paths to make them intersect traps in the return regions. Unlike the previous results, we do not stop the paths at these intersections. Instead we will show how to "bend" them by approximately 90° and extend them along the N-foliation until they leave the thin region. Thus every vertex on the boundary of the thin region is propagated until it leaves the thin region and re-enters a thick piece. This creates new vertices on the thick pieces, and requires these pieces to be remeshed. However, our original meshing of the thick pieces is created using pieces called "sinks". These are designed so that when we remesh the pieces to include the propagated points, no extra boundary vertices are created. Thus the remeshing of the thick pieces ends the construction.

We have two components of the proof to explain: precisely how to propagate points across the thin regions and how to mesh the thick parts so that new vertices can easily be accommodated. The first part is easy (or at least it is an easy modification of what we have already done), so we deal with it first. Later we will define sinks precisely and show how to mesh the thick parts using sinks.

So suppose W is a thin region, i.e., a union of sectors and suppose we are given a collection of vertices of the N-sides of W. We propagate these vertices across the thin parts we did in the proof of Theorem 1.4 using a value $0 < \theta < 60^\circ$ (it will be convenient to assume this value is small at certain points of the proof). In the

proof of Theorem 1.4 we replaced the propagations paths by θ-paths that hit a trap somewhere inside the first return region it enters. For that proof, we wanted the θ-paths to end on a vertex i.e., a point where a trapping edge met the N-side of a thin piece. This was so the θ-paths would form the edges of a mesh.

For the proof of Theorem 1.5 the propagation is exactly the same until the last segment of the θ-path. Instead of choosing the last θ-segment to end at a vertex, we choose it to end at the interior point of a trapping edge. Moreover, different θ-paths should end at distinct points. This is clearly possible because we have chosen $\theta < 60^\circ$ so we can always increase θ a little, make the ending points distinct and still have 60°-paths.

The point of making the endpoints distinct is that we are not going to terminate the θ-path at this point, but are going to "bend" it by approximately 90° so that it becomes a N-segment and leaves the thin part W through an E-side. The precise construction is illustrated in Figure 40. Note that in addition to "bending" the θ-path so that it exits the thin region in the N-direction, we also add two extra N-segments.

The new paths we create can only intersect $O(n)$ other θ-paths. Since we only do this bending construction $O(n)$ times, we create at most $O(n^2)$ new vertices. Thus the thin part W has a quadrilateral mesh with the correct angle bounds and using at most $O(n^2)$ quadrilaterals. The harder part of Theorem 1.5 is to see what happens on the thick parts.

Suppose R is a simply connected region whose boundary is a closed, simple polygonal curve with M vertices. We say R is a sink if whenever we add N vertices to the boundary of R so that $M + N$ is even, then the resulting polygon R' can be meshed by $O(M+N)$ quadrilaterals with all angles between 60° and 120° and no new vertices are added to $\partial R'$. The evenness is required because of Lemma 11.1. Sinks are useful to us because they can be used to stop propagating paths of vertices (we mesh the outside of the sinks using propagating paths that end on the sink boundaries; we can then mesh the insides of the sinks by definition).

We say that a sink conforms to a PSLG Γ if the edges of the mesh we create for R always cover $\Gamma \cap R$, regardless of the number or arrangement of the extra points added to ∂R. In the next section we will prove the following lemmas.

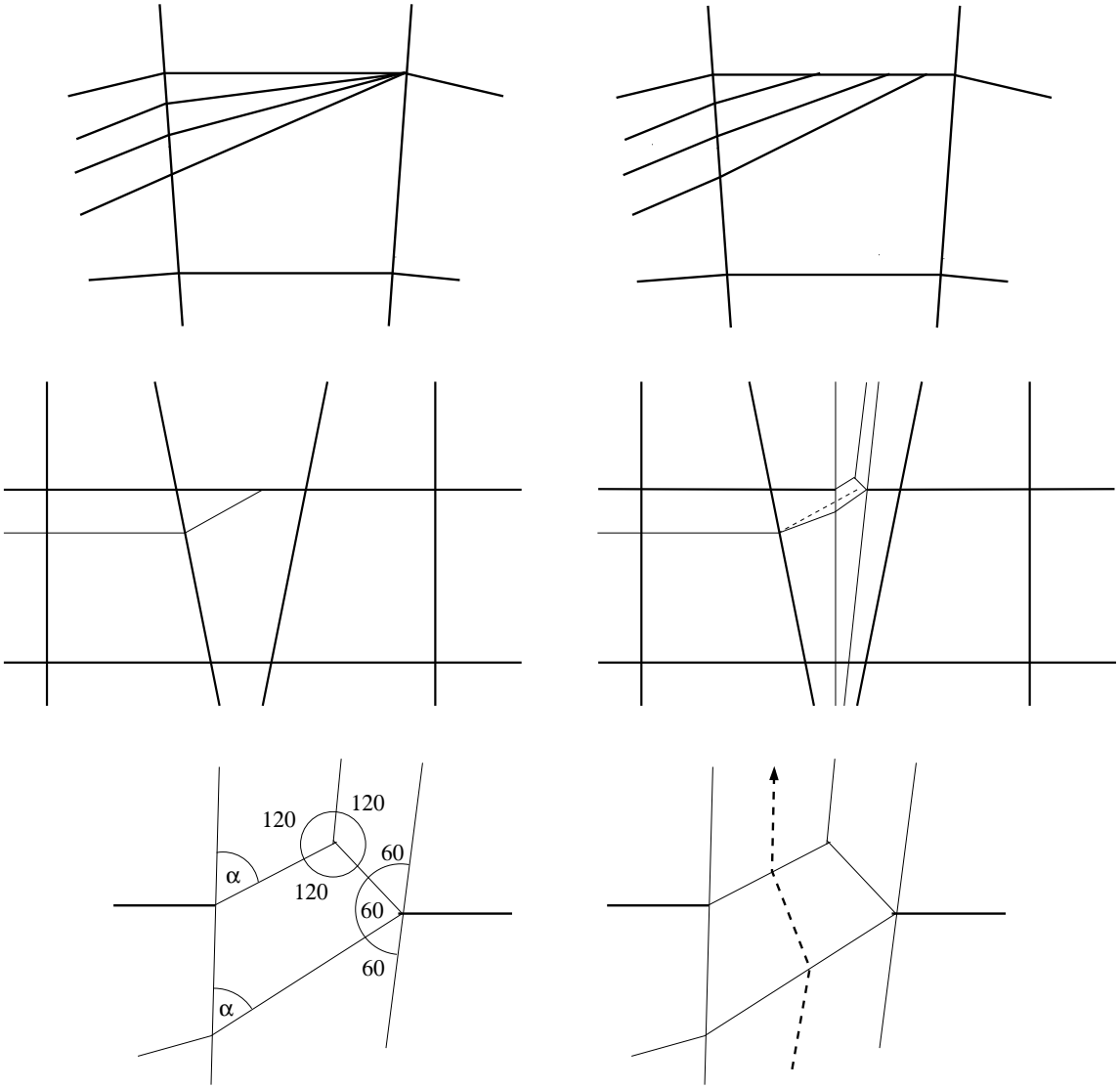

FIGURE 40. The construction in Theorem 1.4 creates paths that end at vertices on the N-sides of thin parts. Since we choose $\theta < 60°$, we can change the final segment of each path so that each path ends at a distinct non-vertices (top pictures). We then apply the construction in the lower pictures; in effect this "bends" the path to become an N-segment that then leaves the thin part and creates two new N-segments as well. The procedure creates only quadrilaterals with angles between 60° and 120°. The left bottom shows an enlargement with the angles labeled. Note that $60° < \alpha < 90°$. If later terminations create a path that crosses the previous construction the path is propagated in the usual way for quadrilateral meshes (right side of bottom figure).

Lemma 12.1. *Suppose Q is a quadrilateral with all angles between 60° and 120°. Then we can add $O(E)$ vertices to the boundary of Q to make it a sink, where E is the eccentricity of Q (the ratio of the longest to shortest side). In particular, if Q has bounded geometry then we only add $O(1)$ vertices.*

Lemma 12.2. *Suppose Γ is a PSLG with n vertices. Then there is a collection of conforming sinks $\{S_k\}$ and inscribed thin parts $\{T_j\}$ so that*

1. *The union of the sinks and thin parts covers the interior of Γ (the union of all bounded complementary components).*
2. *Each collection has $O(n)$ elements.*
3. *If S_k has n_k boundary vertices, then $\sum_k n_k = O(n)$.*
4. *S_k has $O(n_k^2)$ interior vertices. Thus $O(n^2)$ vertices are created in total.*

To prove Theorem 1.5 we assume Γ is connected (apply Lemma 9.2), cover all the vertices by constrained sinks, and consider the connected components of the region not covered by these sinks. Each of these has no small angles (all the small angles were covered by sinks) and is simply connected. We compute the thick/thin decomposition for all the components and let W be the union of the hyperbolic thin parts. Mesh the thick parts of all the components with quadrilaterals whose angles are in $[60^\circ, 120^\circ]$ and that have uniformly bounded geometry (this is possible by [14] since these regions have no small angles). Make each quadrilateral a sink by adding $O(1)$ vertices to each boundary. Then propagate every vertex on ∂W across W as a θ-path (some $\theta < 60^\circ$) creating at most $O(n^2)$ new vertices, until the path terminates on the boundary of a sink. Now double the mesh of W (see Lemma 11.3). This insures every sink has an even number of points on its boundary and the total number of vertices on the boundaries of all sinks is $O(n)$. Finally, mesh all the sinks using at most $O(n^2)$ vertices and creating no new vertices on the boundaries. This gives the desired quadrilateral mesh of Γ and proves Theorem 1.5 (except for the proofs of Lemmas 12.1 and 12.2).

13. Sinks

First we construct a simple kind of sink that we call a circular sink. This example will be included in all the more complicated sinks that are described later.

Lemma 13.1. *Suppose R is the convex hull of $M \geq 8$ points on the boundary of a disk, such that all the interior angles of R are > 120. Then R is sink.*

Proof. Let N be the number of new vertices we want to add to R. Start with a regular octagon and mesh it as shown in Figure 41. Draw a concentric 16-gon outside the octagon and mesh the region between them as shown in Figure 42. Continuing in this way we can clearly mesh any regular 2^n-gon with the desired angles.

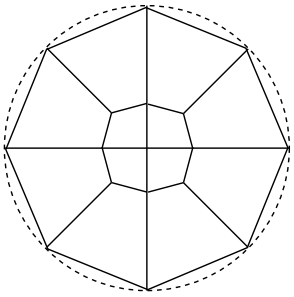

FIGURE 41. The center of the sink.

If $2^k < N < 2^{k+1}$, then we continue this construction up to the 2^k-gon, but at the next level we use the dividing mesh only in $N - 2^k$ of the sectors. In the remaining sectors we simply use segments to connect vertices on opposite sides of the sector. See Figure 43. When we subdivide sectors we have to choose the orientation in each sector so that number of vertices on the sides (1 or 2) matches up correctly. To get them to match all the way around the circle, we see that an even number of sectors must be subdivided, so that an even number of vertices must be added to the outer boundary. The total number of quadrilaterals used is clearly $O(4+8+\cdots+2^{k+1}) = O(M+N)$. In this way we obtain a mesh of convex region W with $N+M$ vertices on a circle, including 8 points forming the vertices of a regular hexagon (hence all the interior angles of our region are $\geq 135°$).

These may not be the points we want, so we place a small copy of W at the center of R and mesh the annular region $R \setminus W$. After a translation and rotation we may assume both circles are centered at the origin and both polygons have a vertex on the positive real axis. Assume the outer circle has unit radius and the inner circle has radius $r = 2^{-120}$. Enumerate the remaining points and suppose $\exp(\theta_k)$ corresponds to $r\exp(\phi_k)$ where we take both arguments in $(0, 2\pi)$. Connect the first point to the second by the polygonal path $2^{-j}\exp(\frac{j}{120}\phi_k + (1 - \frac{j}{120}\theta_k))$ for $j = 0, \ldots, 120$ and add

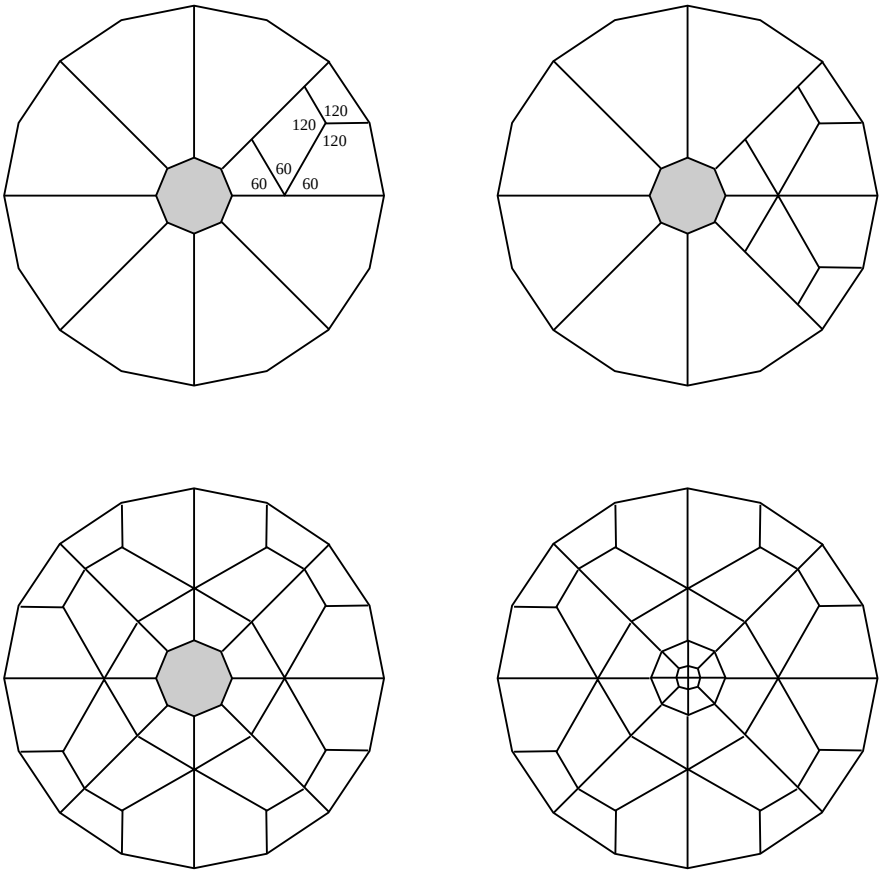

FIGURE 42. The first ring of the sink. The shaded region is the hexagon from Figure 41. We subdivide each sector as shown on the right, then reflect across and edge to subdivide the next sector. Repeat until the whole ring is subdivided. The shaded octagon represents the mesh in Figure 41. We have inserted this figure in the final picture.

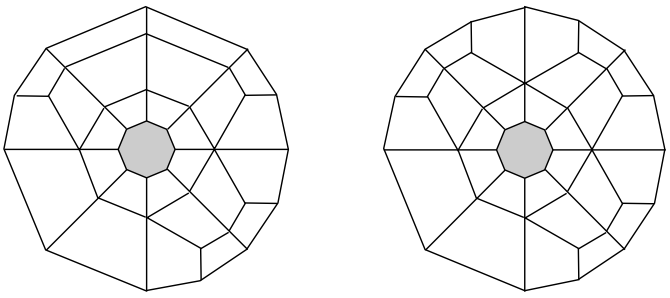

FIGURE 43. We can split just a few of the sectors in a ring. This allows us to place any even number of points on the outer edge.

the closed curves $2^{-j}\exp(\frac{j}{120}\phi_k + (1-\frac{j}{120}\theta_k))$ for $k = 1, \ldots, N+M$. It is easy to see that this forms a quadrilateral mesh of the annular region with all angles between 60° and 120°. See Figures 44 and 45. Thus the total number of quadrilaterals used in this part is $120(N+M)$.

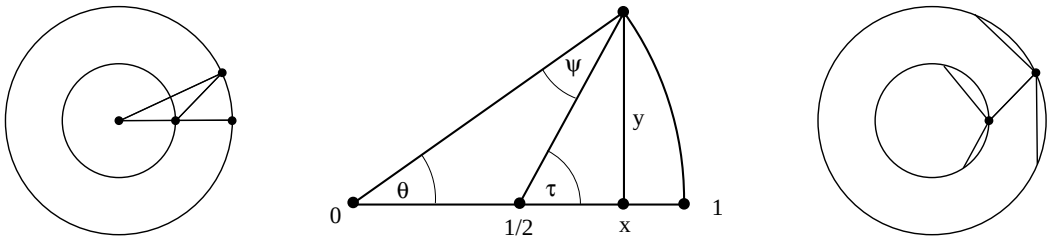

FIGURE 44. If points on circles of radius 1 and $\frac{1}{2}$ have arguments differing by θ then the segment between them makes angles with the radial segments of angles $\psi \le \theta$ and $\tau \le \arcsin(2\theta/(1-\theta^2))$. Taking $\theta = 3^\circ$ insures that $\psi, \tau \le 7.5^\circ$. Thus if we connect two such points, each a vertex of a inscribed polygon with interior angle $\ge 135^\circ$, the four new resulting angles will all be between 60° and 120°.

□

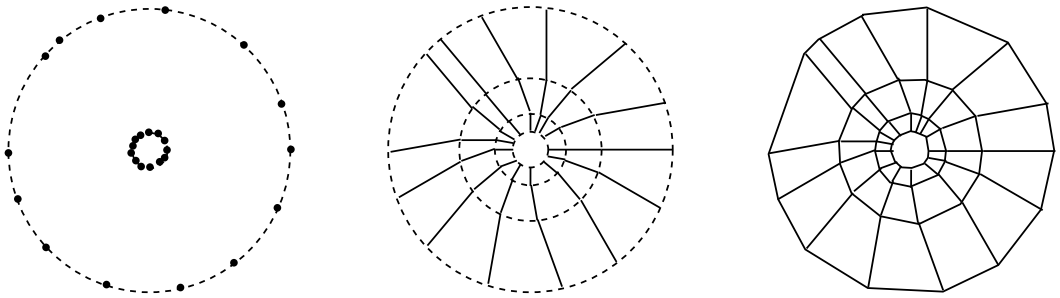

FIGURE 45. Given the same number of points on two concentric circles, we can mesh the annular region between them if the radii have large enough ratio. If we change the arguments slowly enough (e.g., 3° per circle) the angles are all between 60° and 120° (see Figure 44) any argument can be moved all the way around the circle in 120 steps.

Lemma 13.2. *Suppose Q is a quadrilateral with all angles between 60° and 120°. Then we can add $O(\frac{L}{\ell})$ vertices to the boundary of Q to make it a sink (L is the length of the longest side and ℓ is the shortest side).*

Proof. First consider a square. Place a regular octagon at the center and connect it to the edge of square as shown in Figure 46. All vertices on the vertical sides of the square are propagated into the octagon (that we can mesh as a sink by our previous remarks). Next, take this picture, shrink and rotate by 90° and place copies in the shaded squares shown on the right side of Figure 46. Every vertex on the top and bottom edges now propagate either to the central octagon or to one of the smaller octagons insides these squares. Thus the big square is a sink.

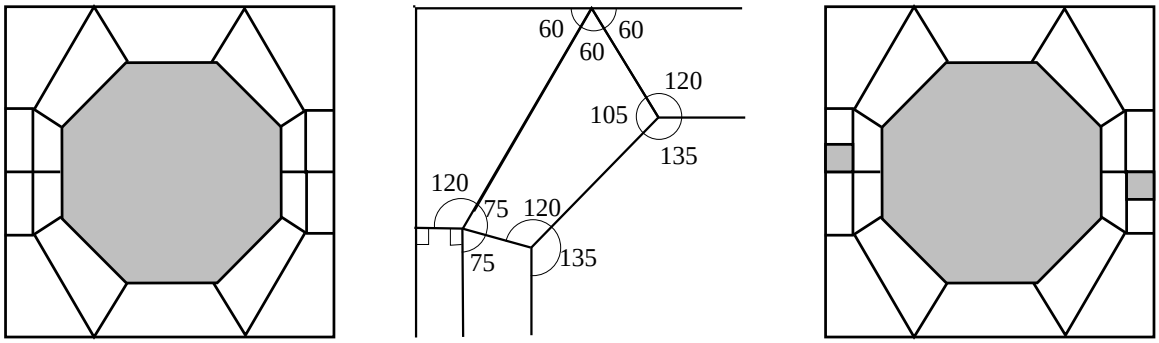

FIGURE 46. The left shows a mesh of the square that is a sink with respect to the vertical sides (in the center octagon we place a circular sink). The angles are detailed in the center. To makes it as sink for the top and bottom edges we place a copy of the first picture, rotated by 90° in the shaded squares on the right.

For an arbitrary $a \times b$ rectangle (assume $a \leq b$), we simply insert squares as shown in Figure 47. If b is not a multiple of a then we add a smaller square and its vertices will have to propagated to the boundary as shown.

FIGURE 47. Making a rectangular sink using square sinks. Every vertex on the outer edge propagates to a shaded rectangle and is "absorbed" by the rectangular sink.

There is a slight problem with evenness. Part of the definition of a sink is that the total number of vertices (original and added) on the boundary must be even. But even if we add an even number of vertices to the boundary of the rectangle, each

subsquare may not get an even number of vertices. See Figure 48. However, it is easy to add extra vertices to the common sides between squares (at most one per side) so that every square has an even number of vertices and hence can be meshed.

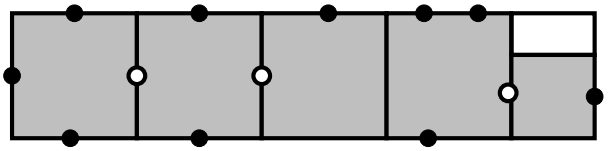

FIGURE 48. Here we have added an even number of vertices to the rectangles (black dots) but some squares get an odd number. We can add at most one vertex per internal edge (the white dots) so that every square has an even number of vertices.

Given a quadrilateral Q and $r > 0$, the interior points that are at least distance r from the boundary form a subquadrilateral Q' with the same angles (at least if r is less than half the inradius of Q). See Figure 49. The region between the quadrilaterals consists of four kites at the corners and four rectangles (shaded). We place a sink in each rectangles and any vertices on the boundary of the inner quadrilateral are propagated until they hit the sink on the other side.

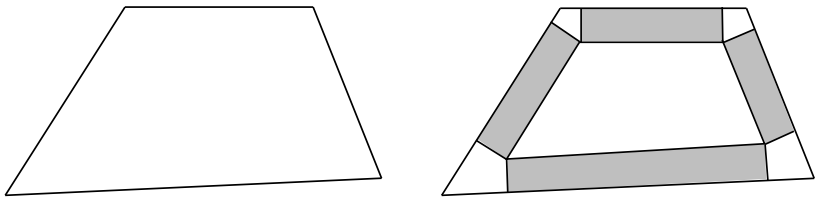

FIGURE 49. Making a quadrilateral sink using rectangular sinks.

As with rectangles, even if we add a even number of vertices to the quadrilateral, some rectangles may get an odd number of vertices (either 0, 2, or all 4). If an opposite pair of rectangles both get an odd number, we connect them with a propagation path giving each one more vertex. See the left side of Figure 50. If two adjacent rectangles get an odd number of vertices, then we add a total of eight vertices as shown on the right of Figure 50.

□

In our earlier construction of circular sinks, four radial lines met at the origin and extended all the way to the boundary of the sink. Now we would like to specify that

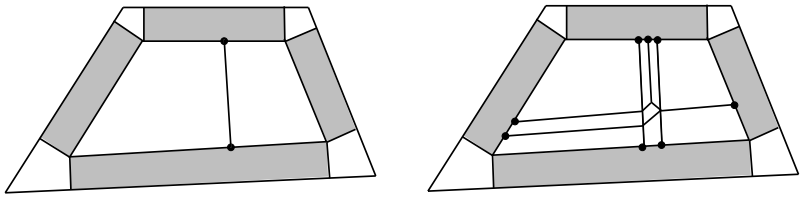

FIGURE 50. We can add internal vertices to make sure every rectangle has an even number of added vertices. If opposite rectangles each need extra vertices we add a propagation path as on the left. If adjacent rectangles need them we use the construction on the right.

k radial segments meeting at v and require the sink's edges to cover these segments. Such a sink will be called a conforming circular sink. See Figure 51.

Lemma 13.3. *Suppose v is vertex with k segments of Γ ending at v. Then given a number s shorter than the distance from v to any other vertex, we can construct a conforming sink with vertices inscribed on the circle of radius $r \leq s/4$ around v. All angles will be in $[60°, 120°]$, except for angles $< 60°$ of Γ at v (these remain undivided). The number of quadrilaterals used is $O(k^2)$.*

Proof. If any of the boundary angles at v is between 120° and 240° we bisect it with a segment of length $s/2$. If any angles are $> 240°$, we trisect it two segments of length $s/2$. Then we bisect each sector using the construction on the right side of Figure 51. The resulting K sectors will be called the basic sectors for v. Note that $K = O(k)$.

Next we cut each sector into smaller regions using the construction shown in Figure 52. Using this construction, each of our basic sectors (that we bisected in Figure 52) are now cut into 4 equal sectors. The extra vertices are propagated along circles centered at the center of the sink. This creates $O(K)$ new vertices, where K is the number of segments in Γ meeting at the vertex at the center of the sink. We can repeat the construction to divide any original sector into 2^m equal sectors. This creates $O(mK)$ vertices. Doing this for all K basic sectors creates $O(mK^2)$ vertices. When we are done, we have meshed a convex region whose vertices are inscribed on a circle around v and the intersection of this circle with each original sector contains 2^m equally spaced points.

We choose a fixed m so that 2^m is larger than the number of vertices on any side of any quadrilateral sink with all angles between 60° and 120° and with eccentricity

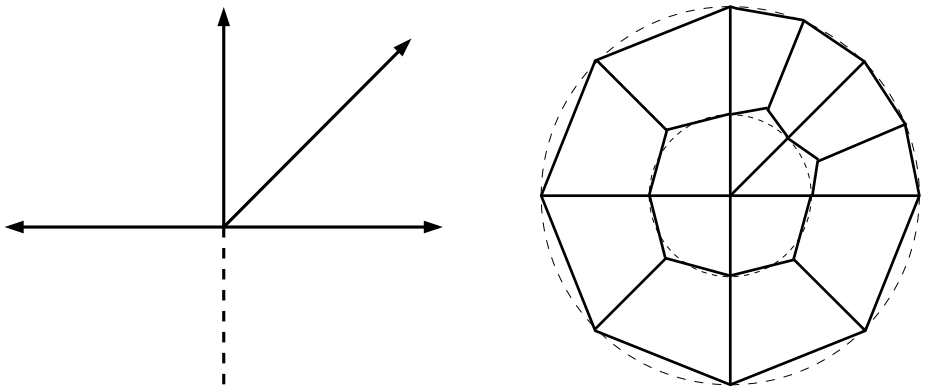

FIGURE 51. If the segments meeting at a point have any angles $> 120^\circ$ we bisect them until all angles are $\leq 120^\circ$. Here we have added the dashed segment. Divide each sector into three quadrilaterals as indicated. The vertices of degree three use only angles of 120°. The other vertices are all on two circles (dashed). This is the first level of bisection.

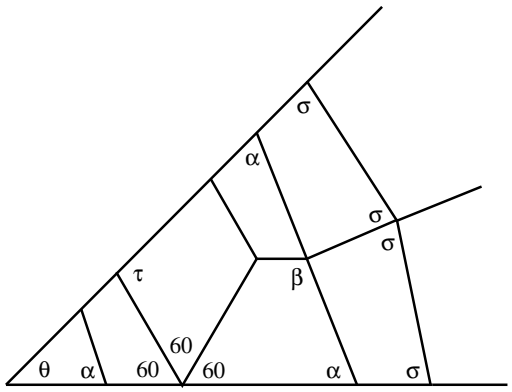

FIGURE 52. A sector of angle $\theta \leq 60^\circ$ is bisected. The marked angles are $\alpha = 90^\circ - \theta/2$, $\beta = 180^\circ - \alpha = 90^\circ + \theta/2$, $\sigma = 90^\circ - \theta/4$ and $\tau = 60^\circ + \theta$. All of these and their supplementary angles lie in between 60° and 120°.

at most 10. This number is uniformly bounded by Lemma 13.2. We then carry out the construction in Figure 53 m times in each of the K basic sectors, to get a mesh of a convex region inscribed in a circle C_0 around v. This circle is represented by the dark shaded circle in Figure 54. Outside this circle we form K disjoint annuli, one corresponding to each sector. The width of the annulus is chosen so that the four intersection points of the annulus boundary with the sides of the sector form a

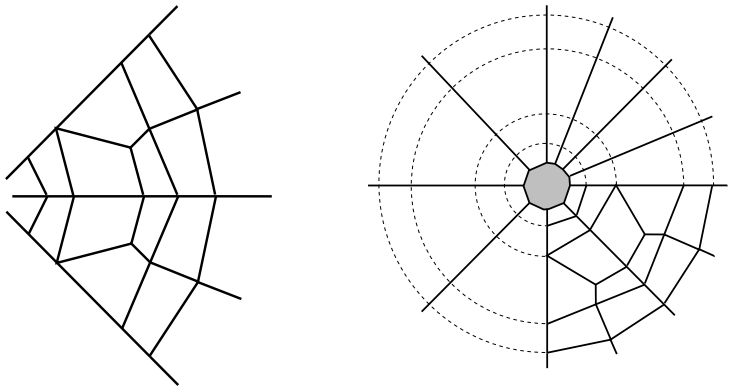

FIGURE 53. On the left is the mesh from Figure 52, together with a reflection across one side. This can be used to mesh a pair of equal angle sectors as shown on the right. The edge vertices for adjacent pairs can be chosen to match, so all K pairs can be meshed with $O(K)$ edges. This is the second and higher level of bisection. Figure 52.

quadrilateral of eccentricity < 10 (this is clearly possible). The outermost circle is denoted C_1.

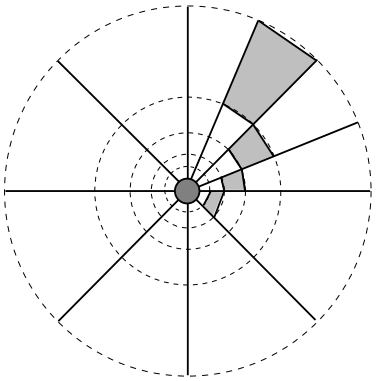

FIGURE 54. The dark disk represents the part of the mesh constructed earlier. In this final stage quadrilaterals are formed from the intersections of basic sectors and annuli and these are filled with sinks. Any vertex on the outer edge C_1, will propagate to one of these quadrilateral sinks. Figure 52.

Inside each such quadrilateral we place a quadrilateral sink, as constructed in Lemma 13.2. The vertices on the radial sides are propagated around the annulus until they hit the same quadrilateral again. Vertices on the side corresponding to the inner circle of the annulus are connected to points on the circle C_0 in the same sector.

We can do this with non-intersecting segments since our choice of m implies there are enough vertices on C_0 in the sector. Any extra points on C_0 are propagated until they hit the quadrilateral sink. Vertices on the "outer" edge of the sink are propagated radially outward until they hit C_1. There are $O(1)$ of these radial propagation lines per sector, hence $O(K)$ overall. Thus the circular propagation paths from the radial sides of Q each hit $O(K)$ radial segments. Thus $O(K)$ new vertices are created for each Q and hence $O(K^2)$ are created overall. □

Theorem 1.6 is proven by making two modifications to the construction above. First, we subdivide all the hyperbolic thin parts so they have angle $\leq \theta/2$ as we did in the proof of Theorem 1.4. Then all the quadrilaterals formed in the thin parts by θ-paths have angles close to 90° except for the places where we "bend" the curve to become a N-segment, but this only involves $O(N)$ quadrilaterals. The other change is in the conforming circular sinks. After we have subdivided angles $> 120^\circ$ and bisected each of the resulting sectors, we continue to bisect each sector until every sector has angle $< \theta/2$. The new vertices added on the radial boundary of the union of sectors lie on four circles. Moreover, when we do the corresponding construction on other pairs of sectors, we can arrange for the new vertices to be on the same sectors, so the meshes on adjacent pairs match up. If we continue until every sector has angle $\leq \theta$, then at most $O(1/\theta)$ quadrilaterals are created.

We then continue with the construction as before, except that K basic sectors have been replaced by $K + O(\theta^{-1})$ sectors. Thus the total number of quadrilaterals created is $O(K^2 + \theta^{-2})$. However, only $O(K + \theta^{-1})$ have angles outside $[90^\circ - \theta, 90^\circ + \theta]$ (see Figure 53). of the mesh shows that only $O(n/\theta)$ angles outside $[90^\circ - \theta, 90^\circ + \theta]$ are used.

Thus a total of $O(n^2\theta^{-2})$ quadrilaterals are created, all with angles in $[60^\circ, 120^\circ]$, but only $O(n/\theta)$ have angles outside $[90^\circ - \theta, 90^\circ + \theta]$. This proves Theorem 1.6.

14. Final remarks

Theorem 1.1 leaves a gap between the known n^2 lower bound and the $O(n^{2.5})$ upperbound of Theorem 1.1. What is the sharp result? My guess is $O(n^2)$. The proof given in this paper assumes there are $O(n)$ thin parts, $O(n)$ return regions, and each return region intersects $O(n)$ thin parts, i.e., every return region uses almost

all the thin pieces. It is easy to see that no two return regions can intersect exactly the same set of thin pieces (otherwise they would be the same return region), but we need to formulate and prove an estimate that says that distinct return regions either use "mostly distinct" thin pieces or traps in them can be built more efficiently than described in this paper. For example, if a thin part is used in more than one return region, then some of the return regions will be further from the vertex of the thin part and hence we can bend more in these regions than in ones closer to the vertex.

Does the constant have to blow up as $\epsilon \to 0$ in Theorem 1.4? If not then, Theorem 1.1 holds with $O(n^2)$. If it does blow up, is ϵ^{-2} the sharp growth rate?

The Delaunay condition is weaker than requiring nonobtuse triangle, but I have not yet been able to better bound for conforming Delaunay triangulation than for nonobtuse triangulation. Is $O(n^2)$ the sharp bound? Can we show the Delaunay and nonobtuse upper bounds are the same (even if we don't know precisely what it is)?

We proved that every triangulation of a simple polygon has an acute refinement with $O(n^2)$ triangles. This worst case occurs but does our method give a better estimate on average? Can we find natural conditions that imply a linear bound? For example, it easy to see that if a triangulated surface is built using n triangles from a compact set K (angles bounded above 0 and below π, edge lengths bounded above 0 and below ∞), then there is an acute triangulation with $O(n)$ elements and the constant depends only on the set K.

Can we find a polynomial bound for nonobtuse triangulation of a triangulated surface? In our proof we use certain facts about planar geometry to show that the tubes on our return regions are longer than they are wide (at least up to a multiple). A surface with a curvature bound should have a similar estimate, but is anything possible in general?

The argument in Section 2 breaks down if we move from surfaces to more general 2-complexes (a finite union of triangles glued along edges but allowing three or more triangles to meet along an edge). In that case propagation paths become propagation trees (since there may be more than one way to continue a path when we cross and edge) and these trees might not be finite. Can we use a bending construction to make them all finite? What sort of upper bound do we get? Can every 2-complex be nonobtusely triangulated? Acutely triangulated?

Dennis Sullivan has pointed out that the "bending propagation paths" argument in this paper is reminiscent of the well known "C^1 closing lemma" of Charles Pugh in dynamical systems (this says that any C^1 vector field on a closed manifold that has flow lines that return arbitrarily close to some point infinitely often can be perturbed in the C^1 metric to a vector field that has a closed orbit). See [51], [52]. Is there a way to interpret our construction as a closing lemma? The C^2 closing lemma is a famous open problem in dynamics. Is there any connection to what we have done here?

If we examine the proof of Theorem 1.1, we see that we create the conforming Gabriel graph in $O(n^{2.5})$ steps. The techniques of [11] then give a non-obtuse triangulation in $O(n^{2.5}\log n)$ steps. The logarithm occurs because the time needed to build the medial axis for circular arc polygon is bounded by $O(n\log n)$. Since the appearance of [11], Chin, Snoeyink and Wang have shown the medial axis for simple polygon with straight sides can be constructed in time $O(n)$. If this was also true for the circular arc polygons, then the logarithmic term could be eliminated.

The techniques in this paper give better estimates if there is a lower bound on the angles in the PSLG. For example, if all the edges are parallel to a finite number of lines and the minimum angle separation is θ, then there is a nonobtuse triangulation with $O(\theta^{-1}n^2\log n)$ elements. In fact, for this conclusion to hold, we only need the N-sides of the thin parts to be either parallel or have angle $\theta > 0$. Indeed, if edges of the PSLG that are ϵ-close in the sense that $\operatorname{dist}(e,f) \le \epsilon \min(\ell(e),\ell(f))$, are either parallel or lie on lines making angle $\ge \theta$ then there is a nonobtuse triangulation with $O((\epsilon^{-1}+\theta^{-1}\log n)n^2)$ elements.

Appendix A. Lower bounds

Consider $\Gamma = [1,N]\times\{0,\frac{1}{n},\frac{2}{n},\dots 1\}$ consisting of $n+1$ parallel horizontal lines of length $N \gg n$ and distance $\frac{1}{n}$ apart. Add n equally spaced vertices to the top edge. See Figure 55.

Any mesh that has an upper angle bound $\theta < 180^\circ$, has the property that there is a path of edges starting at each point of the top edge and proceeding downward inside a vertical cone of angle θ until it hits the bottom edge. If N is large enough,

then these cones are disjoint and so n^2 new vertices are created. This gives a $\sim n^2$ lower bound for Theorems 1.1, 1.4 and 1.5.

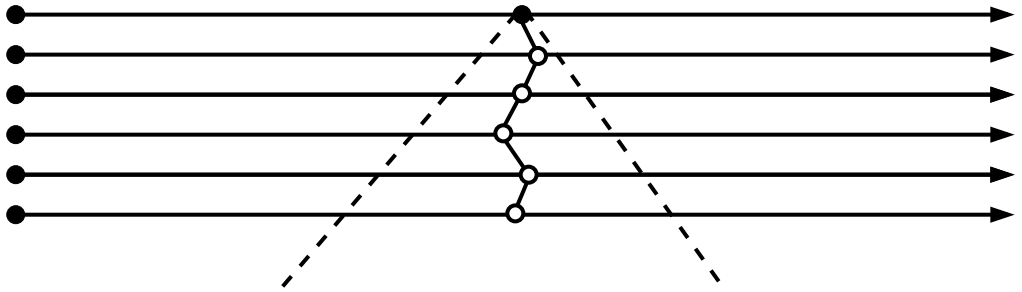

FIGURE 55. At least n^2 vertices are needed when there is an upper angle bound less than 180°.

For Delaunay triangulations put n more vertices on the bottom edge of Γ, directly underneath each of the points on the top edge. Each interval of length 2 in Γ centered above one of these new points v must contain a vertex, because any disk containing this interval as a chord must contain either the point v or the corresponding point on the top edge. See Figure 56. Thus $n(n-1)$ new points are required if $N > 2n$. The same argument works (even more easily) for conforming Gabriel graphs.

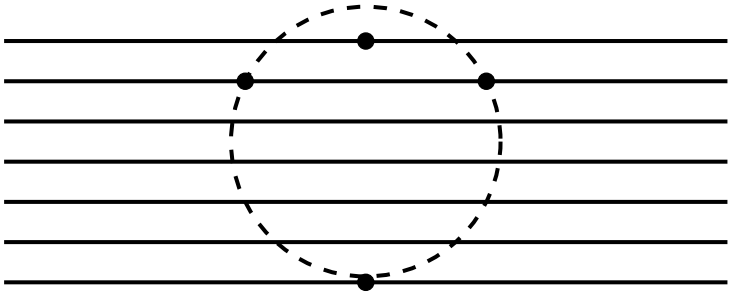

FIGURE 56. Delaunay triangulations for PSLGs require n^2 vertices.

Next we consider β-skeletons for $0 < \beta < 1$. If $v \in V'$ is a point on the top edge, then there must be a vertex on each edge of Γ below it and within horizontal distance $C(\beta)$, for otherwise there is an interval of length $2C(\beta)$ on that edge and v will be with the empty region for this interval, a contradiction. If $N > C(\beta)n$, this shows $n(n-1)$ new vertices are required.

To see that no bound is possible for circle based β-skeletons ($\beta > 1$), suppose V' is a point set whose β-skeleton contains Γ. Suppose I is an interval on the top edge

between two points of V'. If I has length $< \frac{1}{n}\sqrt{\beta^2-1}$ then the intersection of the empty region with the next line is longer than I. See Figure 57. Thus the vertical projection of I onto the second line is strictly contained in an interval J between two points of V' whose empty region strictly contains I, hence the endpoints of I in V'. This is a contradiction, so points of V' on the top edge of Γ are no more than $\frac{1}{n}\sqrt{\beta^2-1}$ apart. Thus there are at least $nN/\sqrt{\beta^2-1}$ such points, a lower bound that we can make as large as we wish for a fixed n and β by taking N large.

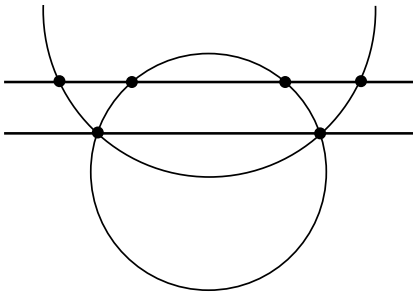

FIGURE 57. For circle based β-skeletons, $\beta > 1$, there is no conforming skeleton with complexity bounded in terms of n.

The Gabriel graph of a point set V contains the minimal spanning tree for V, but there is no bound, depending only on $n = |V|$, for the number of new points needed to make a minimal spanning tree conform to Γ. To see this, note that any conforming spanning tree has length at least nN (the length of Γ) but if it has $|V'|$ vertices then its length can be no more than $N + |V'|$ (take the tree formed with the top edge and connecting each point of V' to the top edge by a vertical edge of length ≤ 1). Thus $|V'| \geq (n-1)N$, which is as large as we wish.

APPENDIX B. APPLICATIONS OF NICE TRIANGULATIONS

As noted in the introduction, nonobtuse triangulations arise naturally as "nice cases" in several numerical methods. Here we list a few to give a flavor of these applications

Discrete maximum principle: Nonobtuse triangulations imply maximum principles ($\sup_\Omega u \leq \sup_{\partial\Omega} u$) for various discrete solutions of PDE's such as discrete

harmonic functions in [22]. In many cases, all that is really needed is a Delaunay triangulation, e.g., [15], [67]. Bounding angles away from 0 and π lead to weak discrete maximum principles ($\sup_\Omega u \leq C \sup_{\partial\Omega} u$) as in [57] and numerous other papers.

Condition numbers: In [68] Vavasis gives a weak maximum principle for discrete solutions of $\nabla \cdot (c\nabla u) = 0$ and notes that the maximum principle holds for nonobtuse triangulations (citing Wahlbin). Vavasis bounds various matrix norms arising from the finite element method in terms of the number n of triangulation elements; for general triangulations his estimate is exponential in n, but for nonobtuse triangulations it is only linear in n.

Stieltjes matrix: The finite element method leads to consideration of the matrix $\int \nabla\phi_j \nabla\phi_k dxdy$, where $\{\phi_k\}$ is a basis of piecewise linear functions on the triangulation. This matrix is an Stieltjes matrix (symmetric, positive definite, negative off the diagonal) for a nonobtuse triangulation and this leads to faster iterative solutions of the corresponding linear system (see [60]). Alternative fast methods are available for more general triangulations, e.g., [16], but are more involved.

Dual graphs: The dual graph of a nonobtuse triangulation can be constructed by simply connecting the circumcenters of adjacent triangles. The resulting segments are perpendicular to the boundary and define the edges of the Voronoi diagram of the triangulation vertices. The cells of the Voronoi diagram are used in the "finite volume" method and nonobtuse triangulations lead to a convenient decomposition. See [10].

Edge flipping: First order Hamilton-Jacobi equations $u_t + H(\nabla u) = f(x)$ are numerically modeled in [3] using an update method that behaves poorly if the vector $\nabla H(\nabla u)$ is close to parallel to a triangulation edge. If the triangulation is acute, then adjacent triangles form a convex quadrilateral and the offending edge can be swapped for the other diagonal, often eliminating the near parallelism and giving better numerical results. This paper also contains a maximum principle requiring a nonobtuse triangulation.

Fast Marching Method: The fast marching method ([58]) for solving the Eikonal equation was originally stated for rectangular meshes but adapted to triangular meshes in [42] where it is applied to compute geodesics on triangulated surfaces. The method is simplest and most efficient if the triangulation is acute.

Meshing space-time: The tent pitcher algorithm of [63], [23], [62] constructs meshes in space-time using 1-Lipschitz graphs that are piecewise linear over a planar triangulation. When the triangulation is a acute a simple greedy process always works, but in general a more complicated method is needed to avoid "getting stuck".

Computer learning: In the introduction we noted how nonobtuse triangles arise in the nearest neighbor learning model of [55].

PL approximations: Suppose u is in the Sobolev space $H^2(\mathbb{R}^2)$ and T is a triangulation of $\mathbb{R}^2$. Babuška and Aziz showed in [1] that there is a piecewise linear function v on the triangulation so that $\|u-v\|_{H^1} \leq C\|u\|_{H^2}$ with constant depending on the maximum angle in the triangulation (and blowing up as this angle approaches π). Thus we expect finite element solutions to be good approximations to continuous solutions when the triangulations have angles bounded strictly below 180°.

References

[1] I. Babuška and A. K. Aziz. On the angle condition in the finite element method. *SIAM J. Numer. Anal.*, 13(2):214–226, 1976.

[2] B.S. Baker, E. Grosse, and C.S. Rafferty. Nonobtuse triangulation of polygons. *Discrete Comput. Geom.*, 3(2):147–168, 1988.

[3] T.J. Barth and J.A. Sethian. Numerical schemes for the Hamilton-Jacobi and level set equations on triangulated domains. *J. Comput. Phys.*, 145(1):1–40, 1998.

[4] M. Bern, D. Dobkin, and D. Eppstein. Triangulating polygons without large angles. *Internat. J. Comput. Geom. Appl.*, 5(1-2):171–192, 1995. Eighth Annual ACM Symposium on Computational Geometry (Berlin, 1992).

[5] M. Bern and D. Eppstein. Mesh generation and optimal triangulation. In *Computing in Euclidean geometry*, volume 1 of *Lecture Notes Ser. Comput.*, pages 23–90. World Sci. Publishing, River Edge, NJ.

[6] M. Bern and D. Eppstein. Mesh generation and optimal triangulation. In *Computing in Euclidean geometry*, volume 1 of *Lecture Notes Ser. Comput.*, pages 23–90. World Sci. Publ., River Edge, NJ, 1992.

[7] M. Bern and D. Eppstein. Polynomial-size nonobtuse triangulation of polygons. *Internat. J. Comput. Geom. Appl.*, 2(3):241–255, 1992. Selected papers from the 7th Annual Symposium on Computational Geometry, I (Conway, NH, 1991).

[8] M. Bern and D. Eppstein. Quadrilateral meshing by circle packing. *Internat. J. Comput. Geom. Appl.*, 10(4):347–360, 2000. Selected papers from the Sixth International Meshing Roundtable, Part II (Park City, UT, 1997).

[9] M. Bern, D. Eppstein, and J. Gilbert. Provably good mesh generation. *J. Comput. System Sci.*, 48(3):384–409, 1994. 31st Annual Symposium on Foundations of Computer Science (FOCS) (St. Louis, MO, 1990).

[10] M. Bern and J.R. Gilbert. Drawing the planar dual. *Inform. Process. Lett.*, 43(1):7–13, 1992.

[11] M. Bern, S. Mitchell, and J. Ruppert. Linear-size nonobtuse triangulation of polygons. *Discrete Comput. Geom.*, 14(4):411–428, 1995. ACM Symposium on Computational Geometry (Stony Brook, NY, 1994).

[12] M. Bern and P. Plassmann. Mesh generation. In *Handbook of computational geometry*, pages 291–332. North-Holland, Amsterdam, 2000.
[13] C.J. Bishop. Conformal mapping in linear time. *Discrete and Computational Geometry*. To appear.
[14] C.J. Bishop. Optimal angle bounds for quaderlateral meshes. *Discrete and Computational Geometry*. To appear.
[15] A.I. Bobenko and B.A. Springborn. A discrete Laplace-Beltrami operator for simplicial surfaces. *Discrete Comput. Geom.*, 38(4):740–756, 2007.
[16] E.G. Boman, B. Hendrickson, and S. Vavasis. Solving elliptic finite element systems in near-linear time with support preconditioners. *SIAM J. Numer. Anal.*, 46(6):3264–3284, 2008.
[17] J. Brandts, S. Korotov, M. Křížek, and J. Šolc. On nonobtuse simplicial partitions. *SIAM Rev.*, 51(2):317–335, 2009.
[18] Ju. D. Burago and V. A. Zalgaller. Polyhedral embedding of a net. *Vestnik Leningrad. Univ.*, 15(7):66–80, 1960.
[19] Yu. D. Burago and V. A. Zalgaller. Isometric piecewise-linear embeddings of two-dimensional manifolds with a polyhedral metric into $\mathbf{R}^3$. *Algebra i Analiz*, 7(3):76–95, 1995.
[20] J. Cardinal, S. Collette, and S. Langerman. Empty region graphs. *Comput. Geom.*, 42(3):183–195, 2009.
[21] C. Cassidy and G. Lord. A square acutely triangulated. *J. Recreational Math.*, 13(4):263–268, 1980/81.
[22] P. G. Ciarlet and P.-A. Raviart. Maximum principle and uniform convergence for the finite element method. *Comput. Methods Appl. Mech. Engrg.*, 2:17–31, 1973.
[23] R. Ciarlet-RaviartAbedi, S.-H. Chung, J. Erickson, Y. Fan, M. Garland, D. Guoy, R. Haber, J.M. Sullivan, S. Thite, and Y. Zhou. Spacetime meshing with adaptive refinement and coarsening. In *SCG '04: Proceedings of the twentieth annual symposium on Computational geometry*, pages 300–309, New York, NY, USA, 2004. ACM.
[24] H. Edelsbrunner. Triangulations and meshes in computational geometry. In *Acta numerica, 2000*, volume 9 of *Acta Numer.*, pages 133–213. Cambridge Univ. Press, Cambridge, 2000.
[25] H. Edelsbrunner and T. S. Tan. An upper bound for conforming Delaunay triangulations. *Discrete Comput. Geom.*, 10(2):197–213, 1993.
[26] D. Eppstein. Faster circle packing with application to nonobtuse triangulation. *Internat. J. Comput. Geom. Appl.*, 7(5):485–491, 1997.
[27] D. Eppstein. Beta-skeletons have unbounded dilation. *Comput. Geom.*, 23(1):43–52, 2002.
[28] D. Eppstein, M.T. Goodrich, E. Kim, and R. Tamstorf. Motorcycle graphs: Canonical quad mesh partitioning. *Eurographics Symposium on Geometric Processing 2008*, 27(5), 2009.
[29] H. Erten and A. Üngör. Computing acute and non-obtuse triangulations. In *CCCG 2007, Ottawa, Cananda*. 2007.
[30] H. Erten and A. Üngör. Quality triangulations with locally optimal Steiner points. *SIAM J. Sci. Comput.*, 31(3):2103–2130, 2009.
[31] M. Gardner. Mathematical games. a fifth collection of brain-teasers. *Scientific American*, 202(2):150–154, 1960.
[32] M. Gardner. Mathematical games. the games and puzzles of Lewis Carroll, and the answers to February's problems. *Scientific American*, 202(3):172–182, 1960.
[33] J. L. Gerver. The dissection of a polygon into nearly equilateral triangles. *Geom. Dedicata*, 16(1):93–106, 1984.
[34] M. Goldberg and W. Manheimer. Elementary Problems and Solutions: Solutions: E1406. *Amer. Math. Monthly*, 67(9):923, 1960.
[35] C. Green. Quadrilateral meshes for polgyons with holes. 2010. Preprint.

[36] T. Hangan, J. Itoh, and T. Zamfirescu. Acute triangulations. *Bull. Math. Soc. Sci. Math. Roumanie (N.S.)*, 43(91)(3-4):279–285, 2000.
[37] D. Heath and S. Kasif. The complexity of finding minimal Voronoĭ covers with applications to machine learning. *Comput. Geom.*, 3(5):289–305, 1993.
[38] J. Itoh. Acute triangulations of sphere and icosahedron. In *Differential geometry (Sakado, 2001)*, volume 3 of *Josai Math. Monogr.*, pages 53–62. Josai Univ., Sakado, 2001.
[39] J. Itoh and L. Yuan. Acute triangulations of flat tori. *European J. Combin.*, 30(1):1–4, 2009.
[40] J. Itoh and T. Zamfirescu. Acute triangulations of the regular icosahedral surface. *Discrete Comput. Geom.*, 31(2):197–206, 2004.
[41] J. Itoh and T. Zamfirescu. Acute triangulations of the regular dodecahedral surface. *European J. Combin.*, 28(4):1072–1086, 2007.
[42] R. Kimmel and J. A. Sethian. Computing geodesic paths on manifolds. *Proc. Natl. Acad. Sci. USA*, 95(15):8431–8435 (electronic), 1998.
[43] E. Kopczynski, I. Pak, and P. Przytycki. Acute triangulations of polyhedra and r^n. Preprint.
[44] S. Korotov and J. Stańdo. Nonstandard nonobtuse refinements of planar triangulations. In *Conjugate gradient algorithms and finite element methods*, Sci. Comput., pages 149–160. Springer, Berlin, 2004.
[45] M. Křížek. There is no face-to-face partition of $\mathbf{R}^5$ into acute simplices. *Discrete Comput. Geom.*, 36(2):381–390, 2006.
[46] J. Y. S. Li and H. Zhang. Nonobtuse remeshing and mesh decimation. In *SGP '06: Proceedings of the fourth Eurographics symposium on Geometry processing*, pages 235–238, Aire-la-Ville, Switzerland, Switzerland, 2006. Eurographics Association.
[47] H. Maehara. Acute triangulations of polygons. *European J. Combin.*, 23(1):45–55, 2002.
[48] E.A. Melissaratos and D.L. Souvaine. Coping with inconsistencies: a new approach to produce quality triangulations of polygonal domains with holes. In *SCG '92: Proceedings of the eighth annual symposium on Computational geometry*, pages 202–211, New York, NY, USA, 1992. ACM.
[49] S. A. Mitchell. Refining a triangulation of a planar straight-line graph to eliminate large angles. In *34th Annual Symposium on Foundations of Computer Science (Palo Alto, CA, 1993)*, pages 583–591. IEEE Comput. Soc. Press, Los Alamitos, CA, 1993.
[50] L. R. Nackman and V. Srinivasan. Point placement algorithms for Delaunay triangulation of polygonal domains. *Algorithmica*, 12(1):1–17, 1994.
[51] C.C. Pugh. The closing lemma and structural stability. *Bull. Amer. Math. Soc.*, 70:584–587, 1964.
[52] C.C. Pugh. The closing lemma. *Amer. J. Math.*, 89:956–1009, 1967.
[53] J. Ruppert. A new and simple algorithm for quality 2-dimensional mesh generation. In *Proceedings of the Fourth Annual ACM-SIAM Symposium on Discrete Algorithms (Austin, TX, 1993)*, pages 83–92, New York, 1993. ACM.
[54] A. Saalfeld. Delaunay edge refinements. In *Proceedings of the third Canadian conference on computational geoemtry*, pages 33–36. 1991.
[55] S. Salzberg, A.L. Delcher, D Heath, and S. Kasif. Best-case results for nearest-neighbor learning. *IEEE Trans. Pattern Anal. MAch. Intell.*, 17(6):599–608, 1995.
[56] S. Saraf. Acute and nonobtuse triangulations of polyhedral surfaces. *European J. Combin.*, 30(4):833–840, 2009.
[57] A. H. Schatz. A weak discrete maximum principle and stability of the finite element method in L_∞ on plane polygonal domains. I. *Math. Comp.*, 34(149):77–91, 1980.
[58] J. A. Sethian. Fast marching methods. *SIAM Rev.*, 41(2):199–235 (electronic), 1999.

[59] J. R. Shewchuk. Delaunay refinement algorithms for triangular mesh generation. *Comput. Geom.*, 22(1-3):21–74, 2002. 16th ACM Symposium on Computational Geometry (Hong Kong, 2000).

[60] D.A. Spielman and S.-H. Teng. Nearly-linear time algorithms for graph partitioning, graph sparsification, and solving linear systems. In *Proceedings of the 36th Annual ACM Symposium on Theory of Computing*, pages 81–90 (electronic), New York, 2004. ACM.

[61] T.-S. Tan. An optimal bound for high-quality conforming triangulations. *Discrete Comput. Geom.*, 15(2):169–193, 1996.

[62] S. Thite. Adaptive spacetime meshing for discontinuous Galerkin methods. *Comput. Geom.*, 42(1):20–44, 2009.

[63] A. Üngör and A. Sheffer. Pitching tents in space-time: mesh generation for discontinuous Galerkin method. *Internat. J. Found. Comput. Sci.*, 13(2):201–221, 2002. Volume and surface triangulations.

[64] E. VanderZee, A.N. Hirani, D. Guoy, and E. Ramos. Well-centered planar triangulation – an iterative approach. In Michael L. Brewer and David Marcum, editors, *Proceedings of the 16th International Meshing Roundtable*, pages 121–138, Seattle, Washington, October 14–17 2007.

[65] E. VanderZee, A.N. Hirani, D. Guoy, and E. Ramos. Well-centered triangulation. *SIAM Journal on Scientific Computing*, 31(6):4497–4523, 2010. Also available as preprint arXiv:0802.2108v3 [cs.CG] on arxiv.org.

[66] E. Vanderzee, A.N. Hirani, V. Zharnitsky, and D. Guoy. A dihedral acute triangulation of the cube. *Computational Geometry: Theory and Applications*, (Accepted, and available online), 2009. Also available as a preprint at arXiv as arXiv:0905.3715v4 [cs.CG].

[67] R. Vanselow. About Delaunay triangulations and discrete maximum principles for the linear conforming FEM applied to the Poisson equation. *Appl. Math.*, 46(1):13–28, 2001.

[68] S. A. Vavasis. Stable finite elements for problems with wild coefficients. *SIAM J. Numer. Anal.*, 33(3):890–916, 1996.

[69] L. Yuan. Acute triangulations of polygons. *Discrete Comput. Geom.*, 34(4):697–706, 2005.

[70] L. Yuan and C.T. Zamfirescu. Acute triangulations of doubly covered convex quadrilaterals. *Boll. Unione Mat. Ital. Sez. B Artic. Ric. Mat. (8)*, 10(3, bis):933–938, 2007.

[71] L. Yuan and T. Zamfirescu. Acute triangulations of flat Möbius strips. *Discrete Comput. Geom.*, 37(4):671–676, 2007.

[72] C. Zamfirescu. Acute triangulations of the double triangle. *Bull. Math. Soc. Sci. Math. Roumanie (N.S.)*, 47(95)(3-4):189–193, 2004.

[73] T. Zamfirescu. Acute triangulations: a short survey. In *Proceedings of the VI Annual Conference of the Romanian Society of Mathematical Sciences, Vol. I (Romanian) (Sibiu, 2002)*, pages 10–18. Soc. Ştiinţe Mat. România, Bucharest, 2003.

C.J. Bishop, Mathematics Department, SUNY at Stony Brook, Stony Brook, NY 11794-3651

E-mail address: bishop@math.sunysb.edu